MANIPULATION OF COLD ATOMS USING AN OPTICAL ONE-WAY BARRIER

by

TAO LI

A DISSERTATION

Presented to the Department of Physics
and the Graduate School of the University of Oregon
in partial fulfillment of the requirements
for the degree of
Doctor of Philosophy

September 2008

University of Oregon Graduate School

Confirmation of Approval and Acceptance of Dissertation prepared by:

Tao Li

Title:

"Manipulation of cold atoms using an optical one-way barrier"

This dissertation has been accepted and approved in partial fulfillment of the requirements for the degree in the Department of Physics by:

Michael Raymer, Chairperson, Physics
Daniel Steck, Member, Physics
Stephen Gregory, Member, Physics
Stephen Remington, Member, Physics
Jeffrey Cina, Outside Member, Chemistry

and Richard Linton, Vice President for Research and Graduate Studies/Dean of the Graduate School for the University of Oregon.

September 6, 2008

Original approval signatures are on file with the Graduate School and the University of Oregon Libraries.

An Abstract of the Dissertation of

Tao Li for the degree of Doctor of Philosophy

in the Department of Physics to be taken September 2008

Title: MANIPULATION OF COLD ATOMS USING AN OPTICAL ONE-WAY BARRIER

Approved: _____

Dr. Daniel A. Steck

This dissertation describes the development of an apparatus that can accommodate many atom-optics experiments, as well as an experimental demonstration of an optical one-way barrier for neutral atoms.

The first part of this dissertation describes in detail the design and implementation of our apparatus. The experiment setup consists of optical systems, vacuum systems, imaging systems, and the related electronics. It is designed to be versatile enough for many cold-atom experiments, including the demonstration of an optical one-way barrier for neutral atoms, quantum measurement on the single-atom level, and the study of quantum chaos using Bose-Einstein condensates.

The second part of this thesis presents the experimental study of an optical one-way barrier for neutral atoms. We demonstrated an asymmetric optical potential

barrier for ultracold ^{87}Rb atoms. The atoms are confined in a far-detuned dipole trap consisting of a single focused Gaussian beam from a fiber laser. The optical one-way barrier consists of two focused laser beams oriented nearly normal to the dipole-trap axis and tuned near the ^{87}Rb D_2 transition. The first beam (main barrier beam) is tuned to work as either a potential well or barrier, depending on the state of the incident atoms. The second beam (repumping barrier beam) pumps the atoms to the barrier state on the reflecting side. We investigated the transmission and reflection dynamics of the atoms in the presence of the one-way barrier, and we verified its capability for increasing the phase-space density of a sample of neutral atoms using the one-way barrier. Our experiment is a realization of Maxwell's demon and has important implications for cooling atoms and molecules not susceptible to the standard laser-cooling techniques.

CURRICULUM VITAE

NAME OF AUTHOR: Tao Li

GRADUATE AND UNDERGRADUATE SCHOOLS ATTENDED:

University of Oregon, Eugene, Oregon, USA
Nankai University, China
Hebei University, China

DEGREES AWARDED:

Doctor of Philosophy in Physics, 2008, University of Oregon
Master of Science in Physics, 2002, University of Oregon
Master of Science in Physics, 2000, Nankai University
Bachelor of Science in Physics, 1997, Hebei University

AREAS OF SPECIAL INTEREST:

Atom Optics and Quantum Optics
Quantum Measurement and Quantum Control
Semiconductor Optics and Spintronics
Quantum Information Science and Technology

PROFESSIONAL EXPERIENCE:

Research Assistant:
Atom Optics Lab, University of Oregon, 2004-2008
Semiconductor Optics Lab, University of Oregon, 2003-2004
Mossberg Lab, University of Oregon, 2001-2002
Teaching Assistant:
Department of Physics, University of Oregon, 2000-2003

PUBLICATIONS:

Jeremy J. Thorn, Elizabeth A. Schoene, Tao Li, and Daniel A. Steck, "Experimental realization of an optical one-way barrier for neutral atoms," Phys. Rev. Lett. **100**, 240407 (2008).

Pei-Cheng Ku, Forrest Sedgwick, Connie J. Chang-Hasnain, Phedon Palinginis, Tao Li, Hailin Wang, Shu-Wei Chang, and Shun-Lien Chuang, "Slow light in semiconductor quantum wells," Opt. Lett. **29**, 2291 (2004).

Tao Li, Hailin Wang, N. H. Kwong, and R. Binder, "Electromagnetically induced transparency via electron spin coherence in a quantum well waveguide," Opt. Express **11**, 3298 (2003).

Jian-Guo Tian, Hao-Hua Wang, Wen-Yuan Zhou, Tao Li, Chunping Zhang, and Guangyin Zhang, "Analysis of the influence of thermal effect on Z-scan measurements with nanosecond pulse laser," Chin. Phys. Lett. **17**, 510 (2000).

Tao Li, Jian-Guo Tian, Wen-Yuan Zhou, Chunping Zhang, and Guangyin Zhang, "Cascaded second-order nonlinear effects and all-optical transistor action via cascaded second-order nonlinearities," Physics **29**, 224 (2000).

ACKNOWLEDGMENTS

I would like to take this opportunity to thank those who have given me generous help during the long journey.

I want to thank my advisor: Dr. Daniel Steck. You taught me so much and gave me encouragement, guidance and generous support. I have always been impressed by your understanding of many fields in physics and your excellent technical skills in multiple areas.

I wish to express my appreciation to my co-workers in Steck lab: Jeremy Thorn, Elizabeth Schoene, Peter Gaskell, Aaron Webster, Matthias Fuchs, Yupeng Kong, Eryn Cook, Paul Martin, Rick Montgomery, Sequoia Alba, Ian Kelly-Morgan, Jason Goff, Jamey Davis, Alice Tasker and other people. Working with you guys has always been enjoyable. Particularly I want to thank Jeremy and Libby. Without you guys, I would not have gotten to this point. Best wishes to you guys!

I would like to thank Dr. Michael Raymer: my dissertation committee chair, a great physicist, teacher, and person. I also want to thank Dr. Steven van Enk. I am fortunate to attend group meetings jointly held by the Steck, Raymer, and van Enk groups. The experience of interacting with so many people is unique and valuable.

I want to thank Dr. Hailin Wang and Dr. Thomas Mossberg. Dr. Wang's ability

to find the interesting research topics and to solve puzzles is impressing. I thank Dr. Wang for all his generous help during my tenure in his lab. Dr. Mossberg's attitude toward research and approach to tackling difficult problems left a deep impression on me. I will always appreciate the help from him and all the lab mates I met and worked with.

I appreciate the willingness of five professors to serve on my committee: Dr. Michael Raymer, Dr. Daniel Steck, Dr. Stephen Gregory, Dr. James Remington and Dr. Jeff Cina. They generously devoted their precious time and energy to my thesis and gave me kind help.

I thank Dr. Rudolph Hwa, Dr. John Toner, Dr. Dietrich Belitz and Ms. Iris Moye. Your help will always be remembered. Brandy Todd, Jeff Chang, Bonnie Grimm, Patty Smith, Jani Levy, and other staff are always happy to lend a hand when I ask for help. Kris Johnson, John Businger, David Senkovich, and Jeffery Garman at the machine shop helped me a lot. Thank you!

I thank the fellow graduate students in the physics department for sharing the happiness and depression, especially the guys entered the program the same year as me. I owe a debt of gratitude to Dr. Guoqiang Cui for letting me use his UO thesis LaTeX template and answering my questions.

In the end, I want to thank my family. My parents, my parents-in-law, my wife Dr. Mei Jiang, my brother, and my daughter Tianyi T. Li are always my faithful cheerleaders and the source of my energy. I love you.

To my wife Mei Jiang

our daughter Tianyi T. Li

and our parents

TABLE OF CONTENTS

Chapter Page

LIST OF FIGURES

Figure Page

Figure Page

Figure Page

Figure Page

CHAPTER I

INTRODUCTION

New types of physical behavior happen under extremely cold conditions. Many great discoveries have been found during the process of achieving lower and lower temperatures. There are at least 18 Nobel Prizes given for work related to low temperature physics. The most famous include superconductivity, superfluidity, and Bose-Einstein condensation. Cold-atom physics has been one of the most active fields in low temperature physics thanks to the development of laser cooling and trapping techniques [1, 2, 3]. Ultracold temperatures reduce the complexity of physical systems, such as Doppler broadening in atomic systems, thus allowing more precise and complete understanding of the system. The creation of cold atoms has contributed to research in many fields, such as atom optics [4, 5], atomic clocks [6], quantum information [7], Bose-Einstein condensation [8, 9, 10], and degenerate Fermi gases [11].

Controlling the internal and external degrees of freedom of atoms and molecules has been one of the most important directions of cold-atom physics and atom-optics research [12]. Coherent control of the quantum states of atoms and molecules began with I. I. Rabi, who applied radio-frequency techniques to molecular beams in 1938 [13]. The methods Rabi developed have formed the basis of precision spectroscopy.

Norman Ramsey divided the resonance region into two separated oscillatory-field regions [14], which became the basis of the atomic clock. In Ramsey's separated oscillatory fields method, the atoms pass twice through the oscillating electromagnetic fields. The interference results in much narrower fringes (Ramsey fringes), thus providing more accuracy. In addition to the control of an atoms' internal degrees of freedom, the control of external degrees of freedom is also an important field. This control has been enabled by laser cooling, which can greatly change atomic kinetic energies and has enabled the lowest temperatures ever achieved.

A particular direction in the control of quantum systems has become a new research field: quantum measurement and quantum feedback control [15, 16, 17]. Our lab is interested in developing new methods of laser cooling and trapping and novel approaches to investigate quantum measurement and quantum feedback control. This thesis presents our efforts in implementing an optical one-way barrier, which could lead to a general method to cool atoms and molecules not amenable to ordinary laser-cooling techniques.

1.1 Overview

There are two major parts to this work. First, we built a fully equipped atom-optics lab starting from scratch. We built mechanical components, electronic equipment, optical systems, a vacuum chamber, and a computer-driven control system. We developed a highly flexible apparatus, which should be able to

accommodate many potential projects. Possible experiments include single-atom-based quantum measurement, study of quantum chaos via Bose-Einstein condensates, and probing the Casimir-Polder force. Second, we carried out the optical one-way-barrier experiment. This experiment is important in several ways: it opens the door to new potential methods to cool atoms and molecules; and it is also a physical realization of Maxwell's demon, which is one of the most intriguing subjects in physics.

1.2 One-Way Barrier

A one-way barrier or "atom diode" is a laser device that lets atoms pass through in one direction but not in the opposite direction. In 2004 and 2005, two research groups independently proposed the concept of the one-way barrier from different standpoints [18, 19]. Ruschhaupt and Muga presented a model for an atom diode that can be realized with adiabatic transfer achieved with lasers [19]. The atom diode is a basic control element in atom-optic circuits and "atomtronics," a new field that focuses on atomic analogies of electronic materials, devices, and circuits [20, 21]. Raizen *et al.* proposed a model of asymmetric optical barriers for atoms, which can be used to compress the phase-space volume of an atomic sample [18].

The one-way barrier proposed by Raizen *et al.* is based on the idea that the character of the interaction between atoms and a laser beam depends on the laser beam's frequency detuning relative to the atomic transition frequency. If the laser frequency is lower than the atomic transition frequency (red detuning), the interaction

potential is attractive and the atoms are pulled towards the region of high laser intensity. On the other hand, if the laser frequency is higher than the atomic transition frequency (blue detuning), the interaction potential is repulsive and the atoms are pushed away from the region of high laser intensity.

The operation of the one-way barrier involves two laser beams (see Fig. 1.1). Suppose there are two non-degenerate ground states that can be optically coupled to an excited state. If the first laser beam is tuned between the transitions from the two ground states to the excited state, it results in an attractive potential well for the atoms in the lower ground state and a repulsive potential barrier for the atoms in the higher ground state. The second laser beam is tuned on resonance with the optical transition from the lower ground state to the excited state and pumps the atoms into the higher ground state. Suppose an atom in the lower ground state starts on the left-hand side of the barrier and encounters the first laser beam. The first laser beam is attractive for this ground state, so the atom will pass through it. Once the atom is in the reach of the second laser beam, it will be optically pumped to the higher ground state. Since the first laser beam is repulsive for atoms in the higher ground state, the atoms will be forced to stay on the right-hand side of the one-way barrier.

In spite of their tremendous success, standard laser-cooling techniques have serious limitations. These techniques all rely on scattering many photons. This requires a cycling transition, which limits the atoms to a small set of atoms in the periodic table. If there are no closed transitions, near-resonant radiation will optically pump

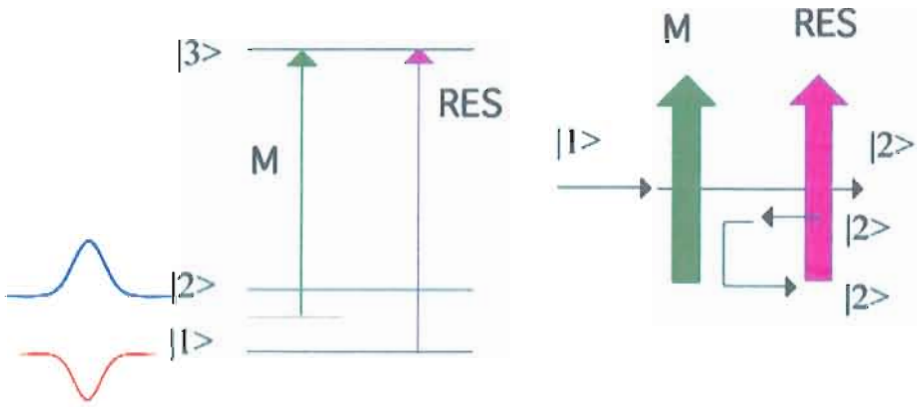

FIGURE 1.1: The simple model of a one-way barrier. The first laser beam M is tuned to the blue of the atomic transition $|2\rangle \rightarrow |3\rangle$ and creates a repulsive barrier for atoms in state $|2\rangle$, but an attractive potential for atoms in state $|1\rangle$. The second laser beam RES is tuned to the atomic resonance $|1\rangle \rightarrow |3\rangle$ and pumps the atoms from $|1\rangle$ to $|2\rangle$. Adapted from [18].

the atoms into "dark" states well before they are cooled. The one-way barrier can be used to compress the phase-space density of an ensemble of atoms or molecules, thus cooling them [18]. Spontaneous emission is only used irreversibly to transfer atoms or molecules from one state to another. In principle, cooling techniques based on one-way barriers can work by scattering only a single photon. The requirement of a cycling transition and the problem of dark states are circumvented. In principle, the realization of one-way barriers paves the way for laser cooling of atoms and molecules not applicable to the standard laser-cooling techniques.

1.3 Maxwell's Demon

1.3.1 The Second Law of Thermodynamics

The second law of thermodynamics is a general principle that places constraints on the direction of heat transfer and the attainable efficiencies of heat engines. It is also a fundamental statement about the increase of entropy in the universe.

The second law of thermodynamics traces its origin to French engineer Sadi Carnot. In order to clarify questions about the efficiency of heat engines, Carnot published a booklet entitled *Reflections on the Motive Power of Heat and on the Machines Adapted to Develop this Power* in 1824 [22]. The most important part of this book discussed the ideal heat engine (Carnot engine). Carnot showed the efficiency of the ideal heat engine is a function only of the two temperatures of the reservoirs between which it works. No heat engine can deliver more work than the ideal heat engine, given the same operating temperatures. Carnot's theory was an early insight into the second law of thermodynamics.

Irish physicist William Thomson (Lord Kelvin) and German physicist Rudolf Clausius became aware of Carnot's work in 1850. At that time, the first law of thermodynamics (conservation of energy) was already established. Combining the first law and Carnot's work, they formulated different statements of the second law of thermodynamics. Clausius' statement of the second law is as follows: "It is impossible to devise an engine which, working in a cycle, shall produce no effect other than the

transfer of heat from a colder to a hotter body [22]." Kelvin's statement of the second law is formulated as follows: "It is impossible to produce work in the surroundings using a cyclic process connected to a single heat reservoir [22]." These two statements are equivalent. In 1865, Clausius introduced the concept of entropy [22]. The second law can also be phrased as "the entropy of an isolated system can never decrease."

Many devices have been concocted that apparently violate the second law, but physically this cannot be possible. To illustrate this, Feynman analyzed a device consisting of a ratchet and a paddle wheel [23]. The ratchet can only rotate in one direction but is prevented from rotating in the opposite direction by a pawl (see Fig. 1.2). A massless and frictionless rod connects the ratchet to a paddle

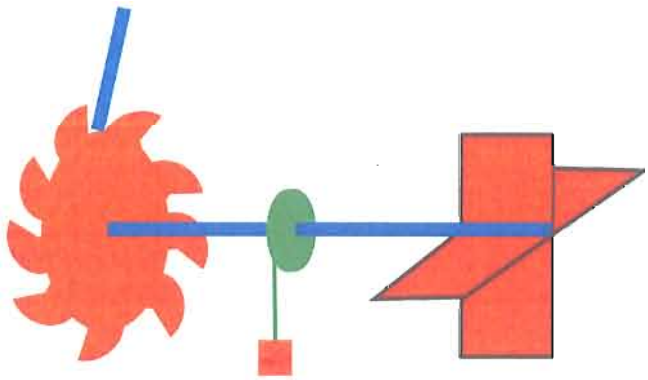

FIGURE 1.2: Feynman's ratchet.

wheel that is immersed in a thermal bath of molecules. When a molecule undergoes Brownian motion and collides with a paddle, it imparts an impulse that exerts a torque on the ratchet. Many random collisions should cause the ratchet to rotate continuously in one direction, since the pawl prevents it from rotating in the opposite

direction. The ratchet's motion can be used to do work. The energy necessary to do the work is from a thermal bath without any thermal gradient, so it contradicts the second law of thermodynamics. Feynman analyzed why the ratchet would fail as an apparent perpetual-motion machine. The ratchet and pawl also experience thermal fluctuations. When the pawl lifts via thermal fluctuations, the ratchet will intermittently reverse, and the ratchet will no longer undergo net directed motion.

1.3.2 Maxwell's Demon

Feynman's ratchet and pawl is analogous to Maxwell's demon. Maxwell's demon is a thought experiment proposed by the Scottish physicist James Clerk Maxwell in 1871 [24]. It was meant to raise questions about the possibility of violating the second law of thermodynamics. Maxwell's demon is a creature that opens and closes a trap door between two compartments of a chamber containing the same gas at equal temperatures (see Fig. 1.3). When a slower-than-average gas molecule flies from the left-hand compartment towards the trapdoor, the demon opens it, and lets it fly into the right-hand compartment. On the other hand, when a faster-than-average gas molecule flies from the right-hand compartment towards the trap door, the demon opens it, and lets it fly into the left-hand compartment. In this way the demon establishes a temperature gradient between the two compartments without doing any work. However, this interpretation is in violation of the second law of thermodynamics.

A variation on Maxwell's demon allows all molecules moving in one direction to go

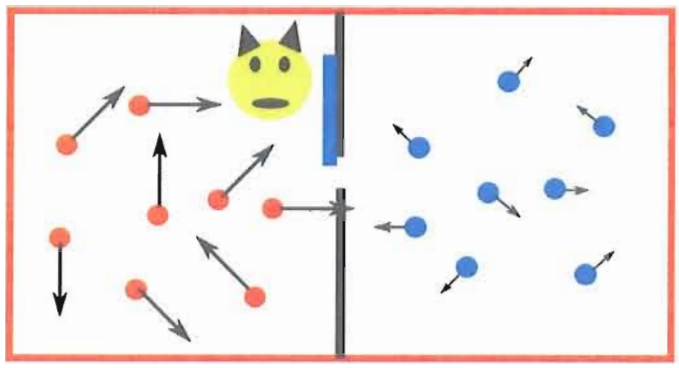

FIGURE 1.3: Maxwell's demon.

through, and prevents the molecules from moving the other way, producing a pressure difference. The pressure gradient can be used to do work, which also seems to violate the second law of thermodynamics. The one-way barrier experiment described in this thesis is a literal realization of this "pressure demon."

Many theories and arguments were proposed to exorcise Maxwell's demon. The information of the demon is the key to reconcile the demon's action with the second law of thermodynamics. One of the most famous theories was presented by Szilard in 1929 [25]. Szilard pointed out that the demon would need to have some means of measuring molecular speed, and the information acquiring would cost energy. The expenditure of energy by the demon will cause an increase in the entropy of the demon, which will be larger than the decrease of the entropy of the gas. Szilard's analysis was still unclear about whether or not the act of measurement must involve an increase in entropy. Landauer later analyzed the thermodynamic cost of elementary information manipulations [26]. He found that almost any operation can in principle

be done in a reversible way and without entropy cost. Landauer's observation shows that the measurement does not necessarily involve an increase of entropy. Bennett made an explicit connection between Landauer's theory and the paradox of Maxwell's demon by proposing that the demon can acquire the information of molecules without doing any work or increasing any entropy in the environment [27]. However, the information must be stored in the demon's memory. To complete a thermodynamic cycle and bring the system to its original state, the demon must reset or "erase" its memory. The erasure operation is thermodynamically irreversible and will increase the entropy in the environment, as required by the second law. This completes the physics of Maxwell's demon.

1.4 Thesis Layout

The principal techniques and basic physics of laser cooling and trapping are presented in Chapter II. We start from an introduction of optical forces on atoms, including both spontaneous-emission-induced forces and stimulated-emission-induced forces. These forces are used for laser cooling and trapping atoms. Then we discuss various techniques related to our experiment to achieve colder temperatures, including Doppler cooling and sub-Doppler cooling. At the end of the chapter, we mention the limitations of ordinary laser-cooling techniques and the motivation for developing new and more general laser cooling methods.

The design, setup, and operation of our experiment apparatus are described in

detail in Chapter III. It includes mechanical, electrical, optical, magnetic, vacuum, and computer elements. Some are home-made, including the tunable external-cavity diode lasers, laser control electronics, etc. This chapter starts from optics, then describes the vacuum chamber, electronics, and computer control system.

The theory of the optical one-way barrier is described in Chapter IV. It starts from a model of the optical one-way barrier used in our experiment. Then we present a scheme for laser cooling based on the optical one-way barrier.

Our experimental results are presented in Chapter V. We demonstrated an asymmetric optical potential barrier for ultracold ^{87}Rb atoms. The atoms are confined in a far-detuned dipole trap consisting of a single focused Gaussian beam from a fiber laser. The optical one-way barrier consists of two focused laser beams oriented nearly normal to the dipole-trap axis and tuned near ^{87}Rb D_2 transitions. The first beam (main barrier beam) is tuned to work as either a potential well or barrier, depending on the state of the incident atoms. The second beam (repumping barrier beam) pumps the atoms to the barrier state on the reflecting side. We demonstrated the transmission and reflection dynamics of the atoms in the presence of the one-way barrier. We also verified its capability for increasing the phase-space density of a sample of neutral atoms. Our experiment is a realization of Maxwell's demon and has important implications for cooling atoms and molecules not susceptible to the standard laser-cooling techniques.

Finally, the conclusions are presented in Chapter VI.

CHAPTER II

PHYSICS OF LASER COOLING AND TRAPPING

2.1 Introduction

Laser cooling and trapping has been a major area of study for the past 30 years [28, 29, 30, 31]. Atoms can now be cooled down to unprecedented kinetic temperatures (less than one μK) and held in the middle of a vacuum system for many seconds. Laser cooling and trapping has revolutionized the field of atomic physics, and opened many completely new research fields including atom optics, Bose-Einstein condensation, and precision measurement based on cold atoms. It has also led to many applications, including some astonishingly accurate atomic clocks, high-precision atom interferometers for measuring gravity, and "lasers" made of coherent matter waves. The first demonstration of laser cooling and trapping of neutral atoms by Steven Chu and William D. Phillips in 1985-1986 and the theoretical investigation by Claude Cohen-Tannoudji were acknowledged by the Nobel Prize of Physics in 1997 [32, 33, 1, 2, 3]. A special indication of the success of laser cooling and trapping was the realization of Bose-Einstein condensation with alkali atoms in 1995, which has been considered a holy grail of modern atomic physics. Due to this ground-breaking achievement, Carl Wieman and Eric Cornell at JILA, and Wolfgang Ketterle at MIT

shared the Nobel Prize of Physics in 2001 [34, 35]. In the remaining part of this chapter we review the techniques of laser cooling and trapping of neutral atoms in our experiment. In Section 2, we review optical forces resulting from spontaneous and stimulated emission. Then we describe Doppler cooling and the magneto-optical trap in Section 3. Sub-Doppler cooling is discussed in Section 4.

2.2 The Optical Forces

Laser cooling and trapping is based on the interaction between laser light and atoms. The interaction between light and atoms is consistent with the conservation of energy and momentum. The energy of light ($\hbar\omega$ for a single photon, where ω is the angular frequency of light) changes the internal energy of the atom. The angular momentum of light ($\hbar$ for a single photon) changes the orbital angular momentum l of the atom, as defined by the selection rule $\Delta l = \pm 1$. The linear momentum of light ($p = \hbar\omega/c = \hbar k$ for single photon, where k is the wave vector of light) will change the momentum of the atoms instead of the internal degree of freedom of atoms. The momentum exchange between the light field and the atoms results in a force exerted on the atoms that can be used to cool and trap them.

After the atom absorbs light, it makes a transition to the excited state, and then returns back to the ground state either by spontaneous or stimulated emission. The optical force arising from spontaneous emission is called the "radiative optical force," "radiation-pressure force," "scattering force," or "spontaneous-emission force." The

optical force arising from stimulated emission is called the "optical dipole force," or "stimulated emission force." Next, we describe these two different forces separately.

2.2.1 Radiative Optical Force

The absorption of light will induce the momentum exchange between light field and atom, thus resulting in a force

$$\mathbf{F} = \hbar \mathbf{k} \Gamma_{\mathrm{p}}, \tag{2.1}$$

where Γ_{p} is the scattering rate of the light. The light will excite the atoms to the excited state. If the light intensity is low enough, they will return to the ground state much more likely via spontaneous emission instead of stimulated emission. Since spontaneous emission is isotropic, the fluorescence light will have momentum $\hbar\mathbf{k}$ in a random direction. In this case the recoil momentum summed over many absorption and spontaneous emission cycles will average to zero. So, the total net force is due to the incoming light and is given by Eq. (2.1). The scattering rate Γ_{p} depends on the light intensity and the frequency detuning from the atomic resonance $\Delta \equiv \omega_{\mathrm{l}} - \omega_{\mathrm{a}}$, where ω_{l} is the laser frequency and ω_{a} is the atomic resonance frequency. Including Doppler effect, the scattering rate Γ_{p} for a two-level atom is given by

$$\Gamma_{\mathrm{p}} = \frac{s_0 \Gamma/2}{1 + s_0 + [2(\Delta - \mathbf{k} \cdot \mathbf{v})/\Gamma]^2}. \tag{2.2}$$

Here Γ is the excited-state population decay rate, the on-resonance saturation parameter $s_0 = I/I_{\mathrm{s}}$ is the ratio of light intensity I to the saturation intensity

$I_s \equiv \pi hc\Gamma/(3\lambda^3)$, and the Doppler frequency shift seen by the moving atoms is $-\mathbf{k}\cdot\mathbf{v}$, where λ is the light wavelength, $\mathbf{k}$ is the wave vector of light, and $\mathbf{v}$ is the atom velocity.

We notice that the force is velocity-dependent, and it can be used to slow down the atoms, thus cooling them. The scattering rate is proportional to the saturation parameter at low intensities, but as the intensity grows it saturates at $\Gamma/2$.

2.2.2 Optical Dipole Force and Optical Dipole Trap

When the detuning is large ($|\Delta| \gg \Gamma$), spontaneous emission is much less frequent than stimulated emission. If the absorption of a photon is followed by stimulated emission into the direction of the same laser beam, then the outgoing photon will take away momentum $\hbar k$, so there is no net momentum transfer. However, if the stimulated emission is into a different direction, there is a redistribution of photons, thus resulting in a force proportional to the difference between the two wave vectors $\Delta\mathbf{k} = \mathbf{k}_1 - \mathbf{k}_2$. If the atom is illuminated with a plane wave, the stimulated emission force will be zero since all the wave vectors are the same. In order to have a non-zero stimulated emission force, there should be a gradient in the light intensity such that the wave vectors point in different directions. This force is also called the optical dipole force [36].

The optical dipole force can be easily calculated from an energy picture or dressed-atom picture. When an atom is put in an inhomogeneous light field, the atom has an energy potential. The potential arises from the atomic energy-level shift in the

light field, called the "light shift." For a two-level atom in a laser beam with Rabi frequency $\Omega = \Gamma\sqrt{s_0/2}$, the light shift is given by

$$\omega_{\rm ls} = (\sqrt{\Omega^2 + \Delta^2} - \Delta)/2. \tag{2.3}$$

The derivation of Eq. (2.3) uses both the dipole and rotating-wave approximations (RWA). For sufficiently large detuning $|\Delta| \gg \Omega$, Eq. (2.3) reduces to $\omega_{\rm ls} \approx \Omega^2/4\Delta = \Gamma^2 s_0/8\Delta$. The light shift $\hbar\omega_{\rm ls}$ can be treated as a potential U in this limit, so the resulting optical dipole force is

$$\mathbf{F} = -\nabla U = -\frac{\hbar\Gamma^2}{8\Delta I_{\rm s}}\nabla I, \tag{2.4}$$

where I is the intensity distribution of light wave.

The optical dipole force is conservative, so it can be used for laser trapping but not for laser cooling. In 1968, Letokhov proposed that the electric field of a laser beam can attract atoms into the regions of high intensity [37]. A trap for small dielectric particles using a laser beam was proposed by Ashkin [38]. The first demonstration of trapped sodium atoms was realized in 1986 [39]. Since then, optical dipole traps have become a widely used tool to manipulate neutral atoms [36]. There are two essential points for an optical dipole trap:

- Sign of the detuning: The sign of the dipole potential is the same as that of laser frequency detuning. Below an atomic resonance (where the laser is red detuned, $\Delta < 0$), the dipole potential is negative and the interaction attracts atoms into the bright area of a light field. Potential minima are found at

positions with maximum light intensity. Above an atomic resonance (where the laser is blue detuned, $\Delta > 0$), the dipole potential is positive and the interaction repels atoms from the bright areas of a light field. Potential minima therefore correspond to minima of light intensity.

- Scaling with intensity and detuning: When the RWA is valid and in the limits of small intensity and large detuning, the optical dipole potential scales as I/Δ, whereas the scattering rate scales as I/Δ^2. Therefore, in order to keep the optical dipole potential deep enough and at the same time the scattering rate as low as possible, optical dipole traps with high intensities and large detunings are used. In our experiment, the optical dipole trap is created by a 1090 nm fiber laser with an output power as high as 20 W, which is far off resonance with the ^{87}Rb D_2 line around 780 nm. Note that the fiber laser is so far off-resonant, the RWA and two-level atom approximation cease to be good approximations, but the dipole approximation still holds.

The simplest optical dipole trap consists of a strongly focused single Gaussian laser beam, tuned far below the atomic resonance frequency. The spatial intensity distribution of a focused Gaussian beam with power P propagating along the z axis is described by

$$I(r,z) = \frac{2P}{\pi w^2(z)} \exp\left(-2\frac{r^2}{w^2(z)}\right), \tag{2.5}$$

where r is the radial coordinate. The $1/e^2$ radius $w(z)$ depends on the axial coordinate

z by

$$w(z) = w_0\sqrt{1+\left(\frac{z}{z_\mathrm{R}}\right)^2}, \tag{2.6}$$

where w_0 is the minimum radius in the plane $z = 0$, called the beam waist, and $z_\mathrm{R} = \pi w_0^2/\lambda$ denotes the "Rayleigh length." In the limit of low intensity, the optical dipole trap potential is proportional to the light intensity. The trap depth is given by $U_0 = |U(r = 0, z = 0)|$.

If the thermal energy $k_\mathrm{B}T$ of the atoms is much smaller than the potential depth U_0, the atoms will be localized in a region radially small compared to the beam waist and axially small compared to the Rayleigh range. Under this condition, the optical dipole potential can be approximated by a simple cylindrically symmetric harmonic oscillator

$$U(r,z) \simeq U_0\left[1-2\left(\frac{r}{w_0}\right)^2-\left(\frac{z}{z_\mathrm{R}}\right)^2\right]. \tag{2.7}$$

The optical dipole trap is characterized by the oscillation frequency ω_r in the radial direction and the oscillation frequency ω_z in the axial direction. The oscillation frequencies can be derived by a Taylor expansion of the optical dipole potential in the radial and axial directions. The harmonic potential is given by

$$U = \frac{1}{2}m\omega^2x^2, \tag{2.8}$$

where m is the atomic mass. The radial dependence of the dipole potential is

$$U(r) = U_0e^{-\frac{2r^2}{w_0^2}} = U_0\left(1-\frac{2r^2}{w_0^2}+\mathcal{O}[r^4]\right), \tag{2.9}$$

where U_0 is the maximum potential, and w_0 is the beam waist radius. Using the aforementioned equations, we get the radial oscillation frequency

$$\omega_{\mathrm{r}} = \sqrt{\frac{4U_0}{mw_0^2}}. \tag{2.10}$$

Axially the optical dipole potential varies as

$$U(z) = U_0 \frac{w_0^2}{w^2(z)} = U_0 \left(1 - \frac{z^2}{z_{\mathrm{R}}^2} + \mathcal{O}[z^4]\right), \tag{2.11}$$

where $z_{\mathrm{R}} = \pi w_0^2/\lambda$ is the Rayleigh length. Accordingly, the axial oscillation frequency is

$$\omega_{\mathrm{z}} = \sqrt{\frac{2U_0}{mz_{\mathrm{R}}^2}}. \tag{2.12}$$

2.3 Doppler Cooling and the Magneto-Optical Trap

The concept of light pressure has been familiar since Kepler used it to explain the tails of comets [29]. The invention of lasers revolutionized the potential for manipulating particles via the mechanical effect of light. In 1975 T. W. Hänsch and A. L. Schawlow proposed the idea of Doppler cooling for free neutral atoms using laser light [40]. At the same time, D. Wineland and H. Dehmelt suggested the same idea of Doppler cooling for trapped ions [41].

The concept of Doppler cooling is simple. Consider the following case: an atom is irradiated by two counter-propagating laser beams as shown in Fig. 2.1. These two laser waves have the same intensity and frequency ω_{l} which is tuned slightly below the atomic resonance frequency ω_{a} ($\Delta \equiv \omega_{\mathrm{l}} - \omega_{\mathrm{a}} < 0$). For an atom at rest, the two

light waves have the same frequency and the two radiation pressure forces balance each other exactly, so the net force is zero. The frequencies of the two light waves for a moving atom are Doppler shifted. The frequency of the counterpropagating wave is shifted closer to the atomic resonance, whereas the frequency of the copropagating wave is shifted further from resonance. Accordingly the radiation pressure force arising from the counterpropagating wave is stronger than that from copropagating wave. The net force is thus opposite to the atomic velocity v and can be written for small v as

$$F \cong \frac{8\hbar k^2 \Delta s_0 v}{\Gamma[1 + s_0 + (2\Delta/\Gamma)^2]^2} \equiv -\beta v, \tag{2.13}$$

where β is a friction coefficient. For $\Delta < 0$, this force is proportional and opposite to the velocity, thus resulting in viscous damping. By using three pairs of counterpropagating laser beams along three orthogonal directions, one can damp the atomic velocity, achieving "optical molasses."

The damping caused by Doppler cooling is accompanied by fluctuations due to spontaneous emission in random directions at random times. These spontaneously emitted photons trade with the atom a random recoil momentum $\hbar k$, creating momentum diffusion described by a diffusion coefficient $D = 4\Gamma_{\rm p}(\hbar k)^2$. The competition between friction and diffusion leads to a steady-state temperature proportional to D/β. For the case of $s_0 \ll 1$, the equilibrium temperature is always larger than a certain temperature limit $T_{\rm D}$, called the "Doppler temperature," which is given by $k_{\rm B}T_{\rm D} = \hbar\Gamma/2$ where $k_{\rm B}$ is the Boltzmann constant and Γ is the decay

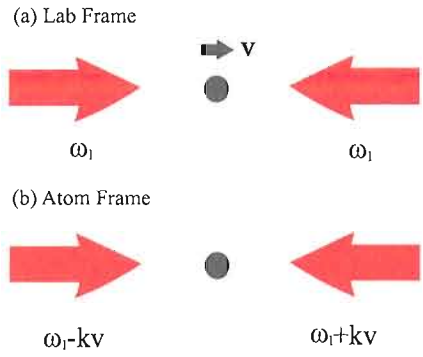

FIGURE 2.1: Doppler cooling in one dimension. The atom is illuminated by two counterpropagating laser beams with the same frequency. The laser frequency detuning is negative, i.e. $\omega_l < \omega_a$, where ω_l is the laser frequency and ω_a is the atomic resonance frequency. Due to the Doppler effect, the atom sees two lasers with different frequencies, thus feeling different radiation pressure forces. This imbalance results in Doppler cooling. The net effect of absorption and spontaneous emission of photons is to slow down the atoms, i.e., to cool them.

rate or natural linewidth of the excited state. This temperature limit is reached when $\Delta = -\Gamma/2$, typically below 1 mK for heavy alkali atoms. In our experiment, we use the D_2-transition of Rb atoms at $\lambda = 780$ nm for laser cooling. The natural linewidth of $\Gamma = 2\pi \times 6$ MHz leads to a Doppler temperature of $T_D = 146\ \mu K$.

The Doppler force is a velocity-dependent force. In order to construct a trap, a position-dependent force is necessary. The Doppler force can be made position-dependent through a spatially inhomogeneous Zeeman shift produced by a magnetic field gradient, as proposed by J. Dalibard [42]. In a one-dimensional configuration, the two red-detuned counterpropagating waves have opposite circular polarizations and are in resonance with the atoms at different positions. This scheme takes advantage of both the linear and angular momenta of photons. It results in a restoring force

toward the center point where the magnetic field is zero. The non-zero value of the red-detuning provides the Doppler cooling. This idea is the basis of the magneto-optical trap (MOT) (Fig. 2.2). Soon afterwards this scheme was extended to three dimensions and demonstrated with Na atoms by Raab et al. in 1987 [42]. The MOT, as a robust, large and deep trap, combines cooling and trapping, has a large velocity capture range ($\sim$ 100 m/s) and remains the workhorse of laser cooling and trapping [43].

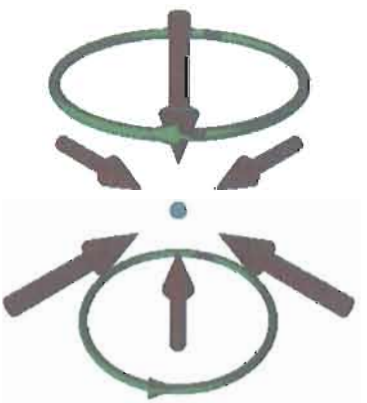

FIGURE 2.2: The configuration of a magneto-optical trap (MOT). It is formed from three orthogonal pairs of laser beams, which have the requisite circular polarization states and intersect at the center of a magnetic quadrupole field created by a pair of coils with opposite currents.

Now we present the principle of a MOT for a one-dimensional configuration (Fig. 2.3). We assume the angular momenta of the ground and excited states of the atoms are respectively $J_g = 0$ and $J_e = 1$. The two counterpropagating waves have the same negative detuning $\Delta = \omega_l - \omega_a$ and opposite circular polarizations. The magnetic-field gradient splits the $J_e = 1$ excited state into three magnetic sublevels.

It is easy to see that the two light waves are in resonance with the atoms at different places. At the center of the trap O, the two forces from the two light waves have the same magnitudes and opposite directions, so the net force is zero (assuming zero velocity). Consider an atom at the left of the trap center O. The σ^+-polarized light, which comes from the left, is closer to atomic resonance with the allowed transition $\mathrm{g} \leftrightarrow \mathrm{e}, m_J = +1$ than for an atom at the trap center O. So the Doppler force increases with respect to that at the trap center O. On the other hand, the Doppler force created by the σ^--polarized light coming from the right decreases with respect to O due to the further frequency detuning from the allowed transition $\mathrm{g} \leftrightarrow \mathrm{e}, m_J = -1$. So the net force for an atom at the left of O points toward the trap center O. The reverse effect happens to the atom at the right of O. Therefore one achieves a stable trapping at O. The total force can by given by

$$F_{\mathrm{MOT}} = \frac{\hbar k \Gamma}{2} \left[\frac{s_0}{1 + s_0 + (2(\Delta - \xi)/\Gamma)^2} - \frac{s_0}{1 + s_0 + (2(\Delta + \xi)/\Gamma)^2} \right], \tag{2.14}$$

where $\xi = kv + \mu' B/\hbar$, and $\mu' B/\hbar$ is the Zeeman shift with $B = B(z) \equiv Az$ and z being the coordinate with respect to O. Here $\mu' \equiv (g_{\mathrm{e}} M_{\mathrm{e}} - g_{\mathrm{g}} M_{\mathrm{g}}) \mu_{\mathrm{B}}$ is the effective magnetic moment. The subscripts g and e refer to the ground and excited states, $g_{\mathrm{g,e}}$ are the Lande g-factors, μ_{B} is the Bohr magneton, and $M_{\mathrm{g,e}}$ are the magnetic quantum numbers. When both the Doppler and Zeeman shifts are small compared to the detuning δ, the force can be written as

$$F = -\beta v - \kappa z, \tag{2.15}$$

which leads to damped harmonic motion of the atoms. The damping coefficient β is

defined in Eq. (2.8). The spring constant κ is given by

$$\kappa = \frac{\mu' A \beta}{\hbar k}. \tag{2.16}$$

The oscillation frequency is given by $\omega_{\mathrm{MOT}} = \sqrt{\kappa/M}$ and the damping rate $\Gamma_{\mathrm{MOT}} = \beta/M$. For magnetic field gradient ≈ 10 G/cm, the oscillation frequency is typically a few kHz, and the damping rate is typically a few hundred kHz.

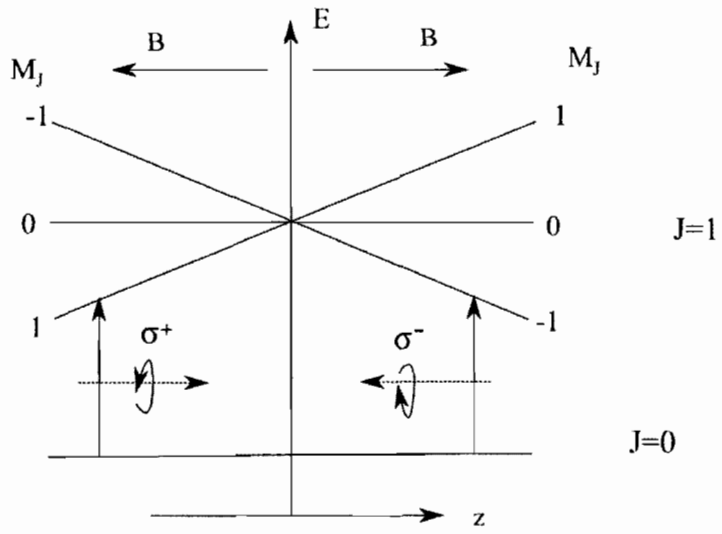

FIGURE 2.3: The mechanism of a one-dimensional MOT for an atom with a $J_{\mathrm{g}} = 0$ and $J_{\mathrm{e}} = 1$ transition. The Zeeman splitting in the magnetic field gradient depends on the atom's position. Two counter-propagating laser beams of circularly-polarized light illuminate the atom. The selection rules for the transitions between Zeeman levels result in an imbalance in the radiative force from the laser beams, pushing the atom back towards the center of the MOT.

In the real world, it is hard to find a $J_{\mathrm{g}} = 0 \rightarrow J_{\mathrm{e}} = 1$ transition. For the D_2-line transitions of an alkali atom with non-vanishing nuclear spin, the ground state $S_{1/2}$ splits into two energy levels, and the excited state $P_{3/2}$ has four levels. The MOT

still works very well for this case. Because of the optical selection rules, the transition from the upper ground state to the highest excited state F level is ideally cycling and used for laser cooling. $\mathbf{F} = \mathbf{I} + \mathbf{J}$ denotes the total angular momentum of the atom, where $\mathbf{I}$ is the nuclear spin, and $\mathbf{J}$ is the total angular momentum of the electron. The energy structure corresponding to different values of F is called hyperfine structure. But due to the finite linewidths, off-resonance excitation, and other hyperfine energy levels, the cycling is not perfect. The hyperfine splitting in the ground state is very large (compared to the laser linewidth and optical transition linewidth), so atoms that decay to the lower ground state are stuck in this "dark" state and are no longer cooled and trapped. In order to prevent this, a second "repump" laser has to be used to transfer atoms from the "dark" lower ground state to the upper one.

In general, the MOT is a very forgiving trap because it is not very sensitive to polarization, intensity, and alignment [28]. The trap is easy to construct, and it can be operated with a room-temperature cell where alkali atoms are captured. The lasers used to produce the MOT light for many alkali atoms can be low-cost semiconductor diode lasers. The magnetic-field gradients required are modest and can be readily made with air-cooled coils. Naturally the MOT has become the workhorse of atom optics and one of the most economical way to cool atoms to temperatures below 1 mK. Normally the intensity of the lasers used to make a MOT should have a saturation parameter $s_0 \sim 1$. The MOT can work with less intensity, but it will be more sensitive to alignment.

The magnetic field in the MOT changes the atomic resonant frequency in a similar way to the Zeeman slowing technique, so the MOT can capture faster atoms than optical molasses. The typical trap depth of a MOT is about a few Kelvins. The lifetime and the atom number density in steady state are limited by the background pressure. A pressure of 1×10^{-10} Torr corresponds to a trap lifetime of tens of seconds [44]. The atomic density inside a MOT is normally limited to $\sim 10^{11}$ cm^{-3} because the fluorescence light emitted by some trapped atoms is reabsorbed by others, thus causing a repulsive force between atoms [45].

2.4 Sub-Doppler Cooling

In 1988, an experiment conducted at NIST showed the temperature of the atoms in optical molasses was much lower than the Doppler cooling limit T_{D} [46]. This observation eventually led to the idea of "Sisyphus cooling" or "polarization-gradient cooling" [47, 48, 49].

The key features of the new cooling mechanism is the inclusion of the multiplicity of atom sublevels, such as Zeeman levels. Optical pumping of the atoms among these sublevels is the basis of the new cooling mechanism. In the simple model of "Sisyphus cooling," there are two counter-propagating laser beams that have orthogonal polarizations. The superposition of the two beams results in a light field with a varying polarization on the wavelength scale along the direction of the laser beams, which is called a "polarization gradient." The light shifts and optical pumping

effects for the ground state Zeeman sublevels depend on the polarization of light, and thus are position-dependent. Atoms at rest have ground-state orientations caused by optical pumping that distribute the populations among the Zeeman sublevels. The ground state orientation reflects the local light field in the presence of polarization gradients. For atoms moving in a light field with a polarization gradient, optical pumping tries to adjust the atomic orientation to the light field with changing polarizations. In the low-light-intensity regime, the orientation of moving atoms always lags behind the orientation for stationary atoms. This nonadiabatic following is essential to the new cooling process.

Consider the laser configuration shown in Fig. 2.4. There are two counter-propagating plane waves with orthogonal linear polarizations and the same frequency and intensity along the z-axis. The polarization of the total field changes from linear to σ^+ circular to orthogonal linear to σ^- circular in the space of every $\lambda/2$.

Now we consider the simple case where the atomic ground state has an angular momentum $J_g = 1/2$. Depending on the laser polarization, the two Zeeman sublevels $M_g = \pm 1/2$ undergo different light shifts, so the Zeeman degeneracy in zero magnetic field is removed. Notice that the polarization gradient behaves similarly to a magnetic field. The spatial modulation of the light shifts of the two sublevels changes with a period of $\lambda/2$, as shown in Fig. 2.4. Consider the $J_g = 1/2 \rightarrow J_e = 3/2$ transition, which is one of the simplest transitions that shows sub-Doppler cooling, the optical pumping due to pure σ^+ light drives the ground-state population to the $M_g = +1/2$

state. This happens because the absorption always produces $\Delta M = +1$ transitions, whereas the subsequent spontaneous emission involves $\Delta M = \pm 1, 0$ transitions. So the net effect is $\Delta M \geq 0$ for each scattering event. For σ^- light the population is pumped to $M_g = -1/2$ state. So the spatial modulation of laser polarization results in a spatial modulation of the optical pumping rate with a period of $\lambda/2$. The atoms need to readjust their population from $M_g = +1/2$ to $M_g = -1/2$ and back again when they travel through a half-wavelength in the light field.

The spatial modulation of the laser polarization causes the spatial modulation of both light shifts and optical pumping rates. If the proper sign of the detuning is chosen, optical pumping will always transfers atoms from the higher Zeeman sublevel to the lower one. Suppose the atoms are pumped to the $M_g = +1/2$ state, and move to the right from the bottom of a valley where the light polarization is σ^+. In moving through the light field, atoms must increase their potential energy and "climb the hill" because the polarization of the light is changing and the state $M_g = +1/2$ is less strongly coupled to the light. After traveling a distance $\lambda/4$, atoms arrive at the place where the light polarization is σ^- and are pumped to $M_g = -1/2$ state which is lower than $M_g = +1/2$ state now. Then again the atoms are at the bottom of a valley and start to climb the hill. In climbing the hill, the atoms lose the kinetic energy to potential energy, and in the optical pumping process the potential energy is dissipated because the spontaneously emitted photon has higher frequency than the absorbed photon. The non-zero value of the optical-pumping time is the key

to Sisyphus cooling. Because of the finite optical-pumping time, there is a time lag between the internal and external states of atoms, and the atoms can climb up the potential hill before absorbing a photon at the top where they have the maximum probability to be pumped to the bottom of a valley. This cooling process brings to mind the character Sisyphus from Greek mythology, who was always rolling a stone up a hill, which is where it gets its name. After each Sisyphus cooling cycle, the total energy E of the atoms decreases by an amount of the order of U_0, where U_0 is the potential well depth. When E becomes smaller than U_0, the atoms will remain trapped in the potential well.

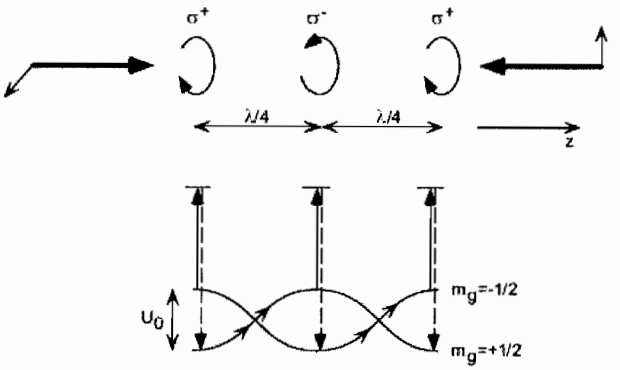

FIGURE 2.4: The principle of Sisyphus cooling. There are two counter-propagating laser beams along the z axis with orthogonal linear polarizations. A spatial polarization gradient with a period of $\lambda/2$ is formed. The spatial modulation of the laser polarization results in spatial modulations of the light shifts of the two ground Zeeman sublevels $M_g = \pm 1/2$. The optical pumping rates between the two sublevels are also spatially modulated. Because of the correlations between the spatial modulations, a moving atom runs up potential hills more frequently than down. The kinetic energy is lost when the atom absorbs laser light at the top of a hill and spontaneously emits a photon of a higher frequency and ends up at the bottom of a potential well. Adapted from [2].

Sisyphus cooling leads to a temperature T_s such that $k_B T_s \simeq U_0$. The potential well depth or the light shift U_0 is proportional to I/Δ. At low intensity, the light shift is much smaller than $\hbar\Gamma$, so it explains why Sisyphus cooling leads to temperatures much lower than those achieved by Doppler cooling, and why the experiment result is much better than the original theoretical prediction.

There are other laser-cooling mechanisms, including sub-recoil cooling and evaporative cooling. They are important to achieve lower temperatures and higher phase-space densities, but they are not directly related to our experiment.

CHAPTER III

EXPERIMENTAL SETUP

This chapter describes the design and construction of our experimental apparatus, which was a major part of the work presented here. Our experimental system was developed from scratch, starting with nothing more than an empty lab.

One of the characteristics of atom-optics experiments is the amount of equipment needed. There are dozens of optical components (mirrors, lenses, waveplates, etc.), nine lasers, tens of electronic-control boxes, miscellaneous electronic equipment (oscilloscopes, function generators, frequency counters, power supplies, transformers, etc.), and all kinds of vacuum pumps (turbo pump, ion pump, titanium sublimation pump, getter pump, etc.). Many of these items are homebuilt in our lab.

3.1 Overview

Our experimental setup is complicated. Roughly, the setup can be divided into a vacuum chamber, laser systems, magnetic systems, imaging systems, and control electronics. A $12' \times 5'$ optical table holds a vacuum chamber, nine lasers, dozens of electronic and mechanical components, and hundreds of optical components used in our experiment, as shown in Fig. 3.1. Most of the electronics boxes are mounted on four big racks and several small racks. Figs. 3.2 and 3.3 show the racks that

hold the laser electronics, analog and digital boxes, acousto-optic modulator control electronics, and magnetic-coil electronics.

3.2 Vacuum System

When we designed our experimental setup, we wanted to make a versatile apparatus that can be used for many purposes. Bearing this in mind, we selected the double-MOT configuration. Normally, researchers use a Zeeman slower [50] and a MOT or a double MOT [51] to generate Bose-Einstein condensates (BEC). The requirements of large atom number and ultra-high-vacuum conditions are difficult to achieve at the same time. A Zeeman slower occupies much space (1-2 m) and requires a high-temperature oven, so we did not consider it. The double MOT is a very common approach to generate BECs and is widely used in many labs. First, a MOT is loaded in a relatively poor vacuum from a room-temperature vapor, and then the pre-cooled atoms are transferred to an ultrahigh vacuum chamber, where the BEC is created. The "one-way optical barrier" experiment does not have such stringent requirements as BEC experiments have. However, we still benefit from the trap lifetime of many seconds in such an ultrahigh vacuum chamber. We wanted to make sure our setup has general extendability to other potential projects, including future BEC related experiments or few-atom quantum-measurement experiments.

To realize the double MOT system, the vacuum system (Fig. 3.4) was designed to have three parts: a relatively low vacuum chamber ($\sim 10^{-8}$ torr) connected to a Rb

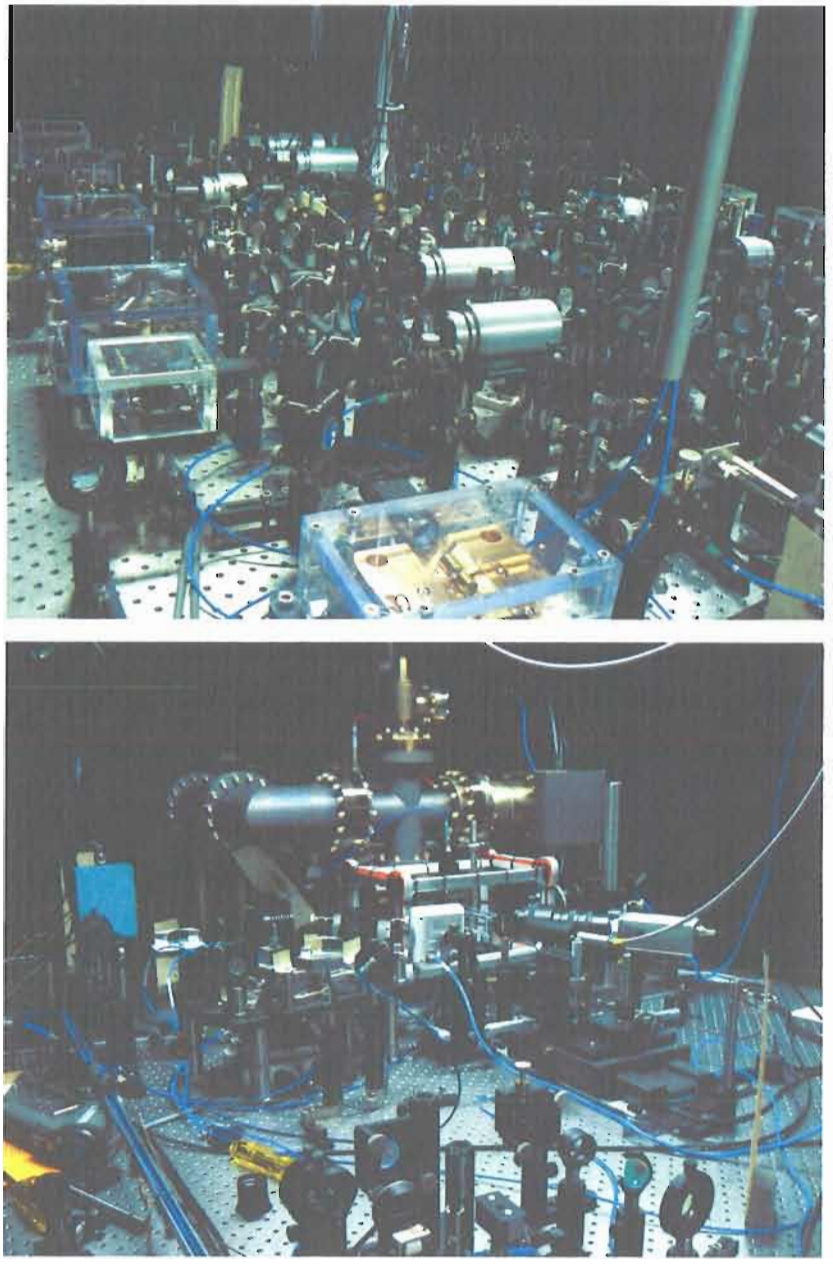

FIGURE 3.1: The optical table. The top image shows the section of table occupied by lasers and optics. The bottom image shows the section of the table occupied by the vacuum chamber and imaging optics.

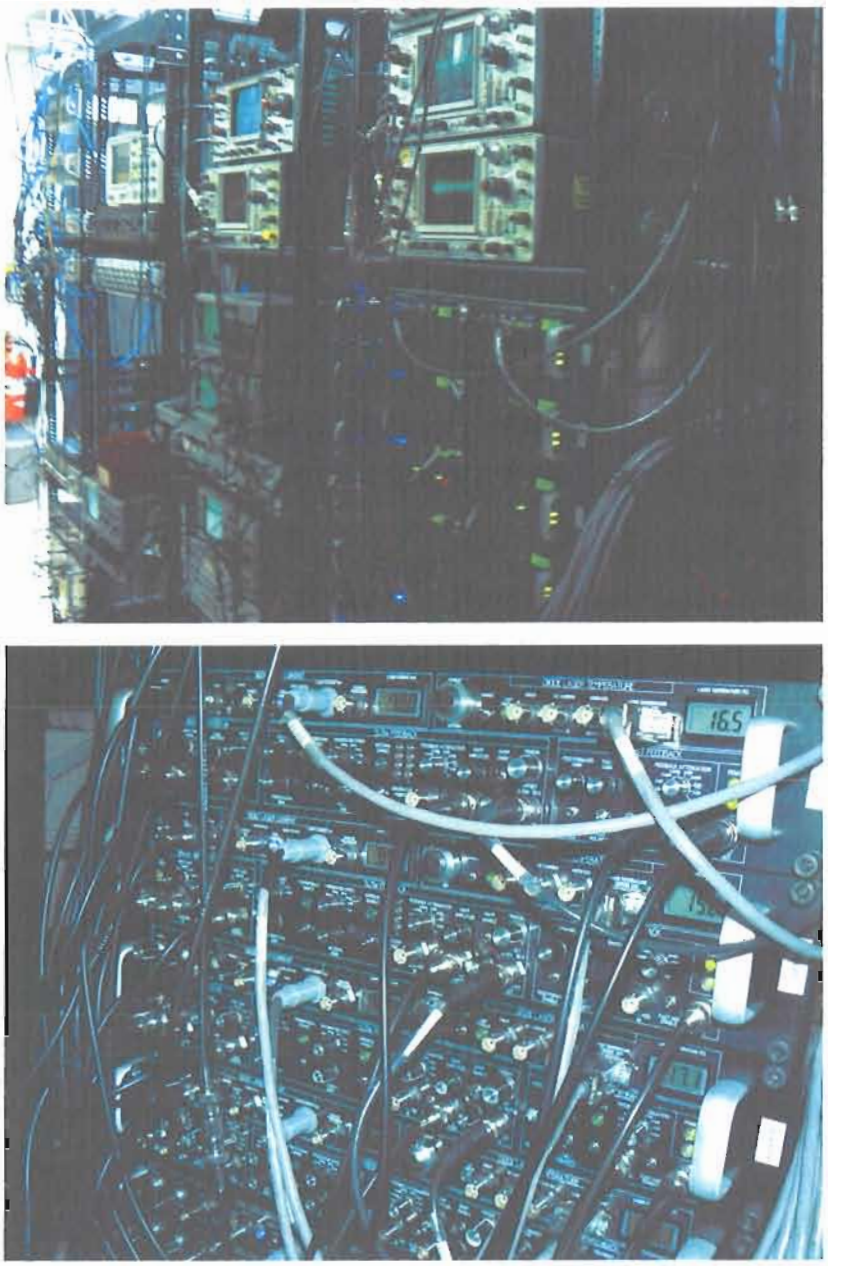

FIGURE 3.2: The electronics racks. The top image shows the racks that hold the laser electronics, analog and digital boxes, oscilloscopes, Fabry-Perot cavity control electronics, and other electronics. The bottom image shows the close-up of the laser-control electronics, including current controllers, temperature controllers, and laser frequency servo-lock boxes.

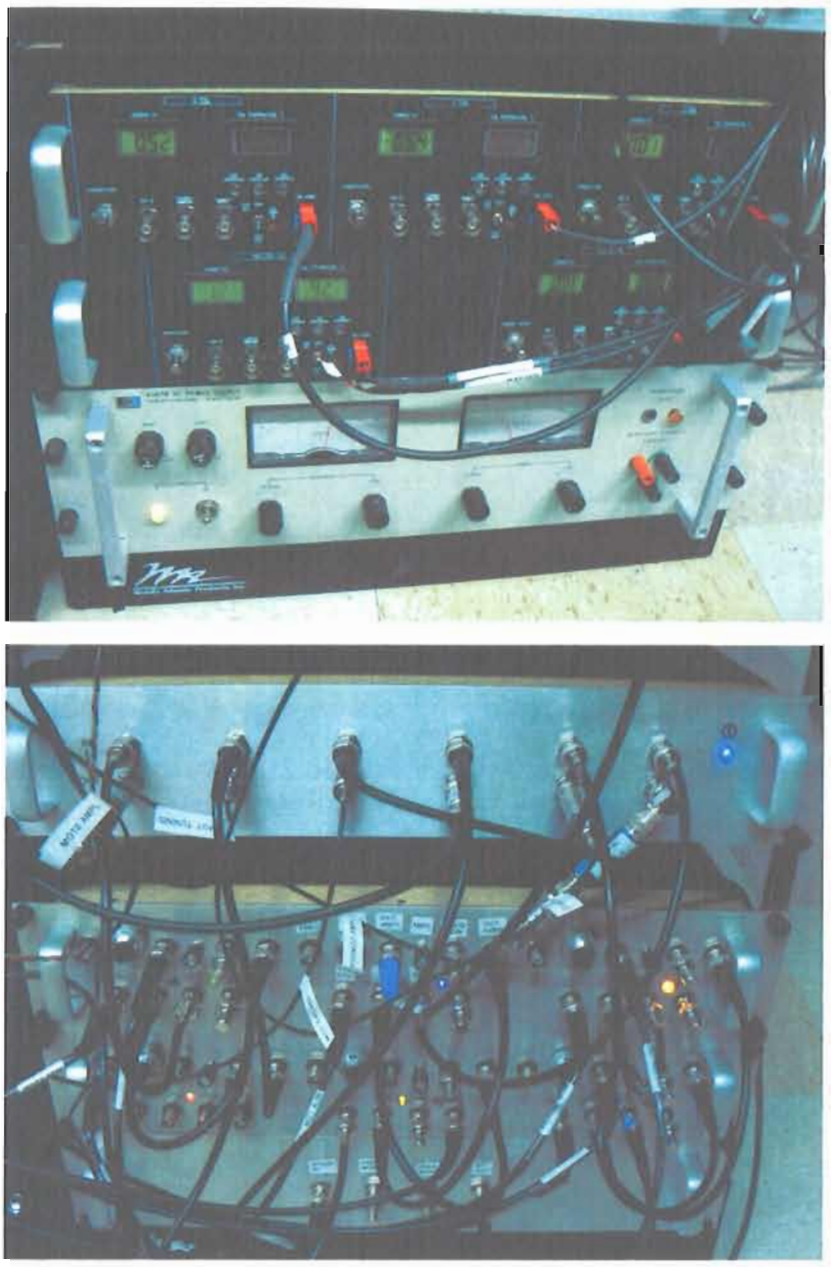

FIGURE 3.3: The electronics racks. The top image shows the racks holding some of the magnetic coil electronics. The bottom image shows the electronics for the AOMs used in our experiment.

ampoule, an ultra-high vacuum (UHV) chamber ($\sim 10^{-11}$ torr) connected to a vapor cell where the experiment is conducted, and a differential pumping tube that connects the two vacuum chambers with very different pressures. A mechanical drawing of the vacuum system (side view) is shown in Fig. 3.5. The higher pressure of the first vacuum chamber allows fast loading of the first MOT from the Rb ampoule. This first MOT functions as a cold-atom source and is constructed using a pyramid MOT design [52]. The pre-cooled atoms are pushed into the second chamber using a laser beam, where a six-beam MOT is formed. We called the first vacuum chamber the pyramid MOT chamber, and the second chamber the science vacuum chamber since the experiment is conducted there.

We use various pumps to achieve the ultra-high vacuum, including a turbo pump backed by a mechanical pump, two ion pumps, a titanium sublimation pump, and several non-evaporable getter pumps. Only the ion pumps are run on a continuous basis. The turbo pump is used only during initial pump down and vacuum bake out. The titanium pump and getter pumps are only activated occasionally, but they operate passively at all times.

Obtaining ultra-high vacuum requires carefully following cleaning, assembly and bake out procedures. Detailed information about working with vacuum systems can be found in an article by Kevin Birnbaum [53].

It is particularly important to avoid contamination of the vacuum system during assembly. When we handle the vacuum parts, we always wear powder-free nitrile

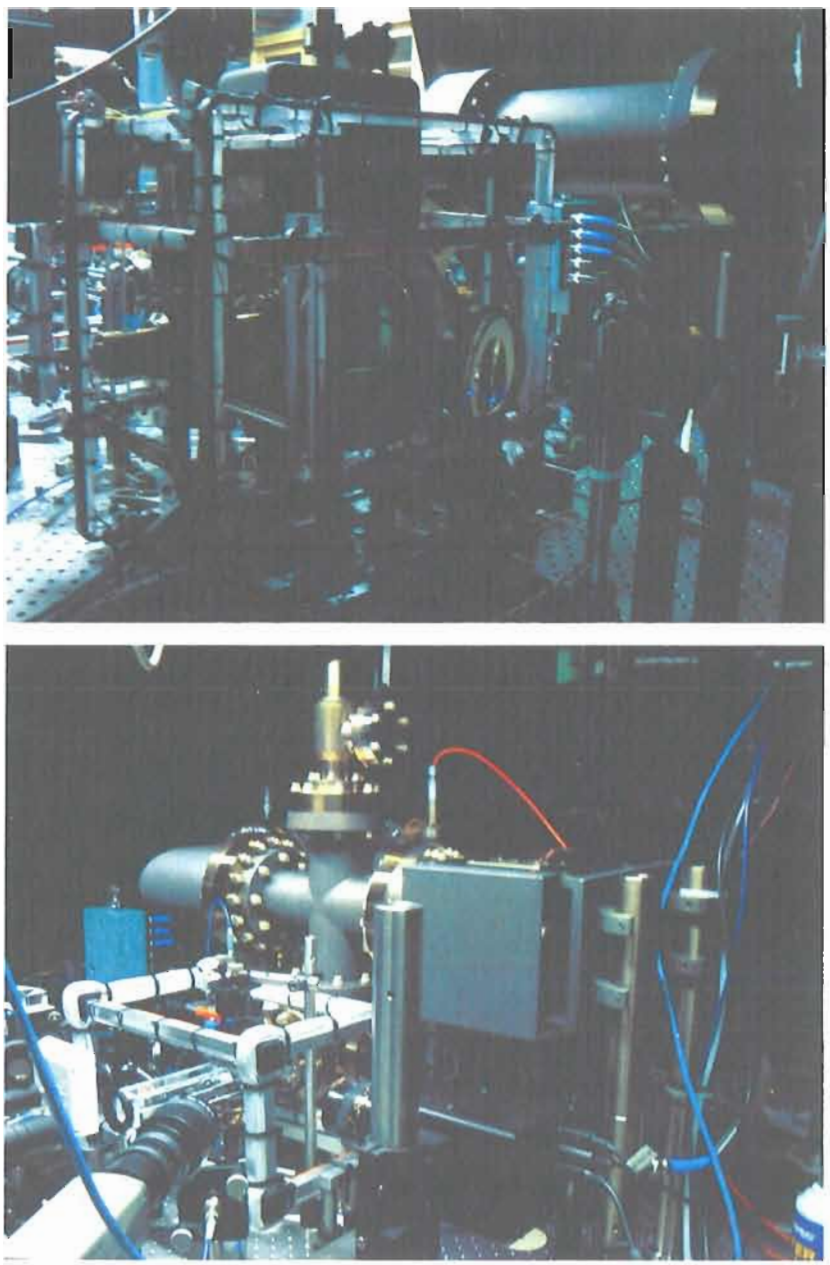

FIGURE 3.4: The vacuum chamber. The top image shows the relatively poor vacuum side (it is still UHV), the 20 L/s ion pump, and the titanium sublimation pump. The bottom image shows the UHV chamber side with the Hellma cell attached and the 75 L/s ion pump. The differential pumping tube can not be seen from these angles.

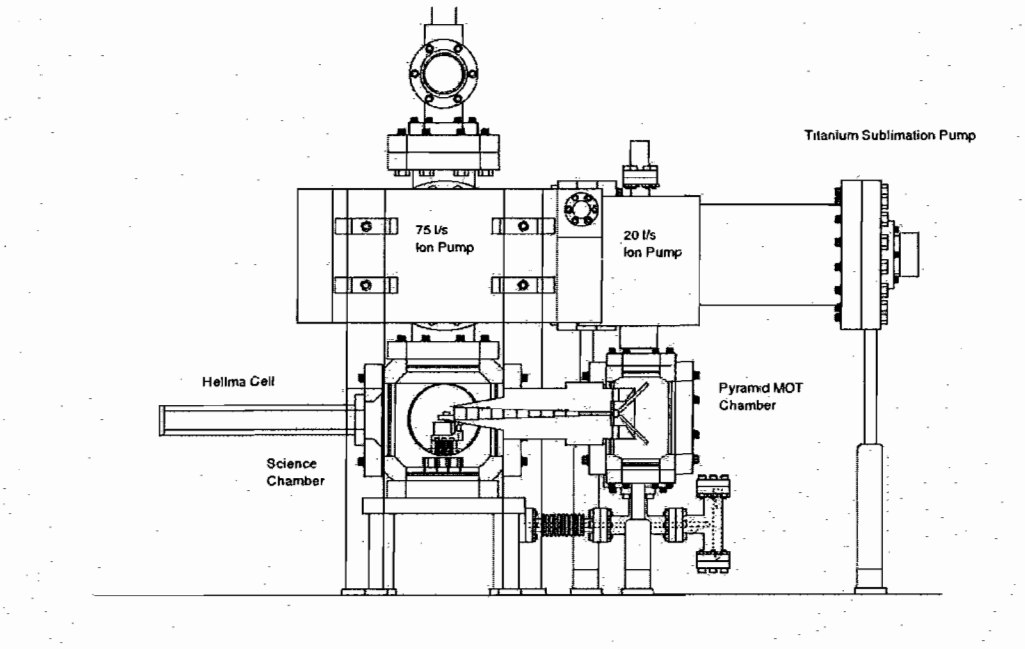

FIGURE 3.5: The mechanical drawing of the vacuum system. The picture shows the Hellma cell, science chamber, differential pumping tube, two ion pumps, titanium sublimation pump, getter pumps, and pyramid MOT vacuum chamber. Adapted from a drawing by D. Steck.

gloves and change them often. Before installation of vacuum parts, we always clean the knife edges and copper gaskets using ultra-pure methanol.

To obtain UHV pressures, the vacuum system must be baked at high temperatures ($\sim$ 200 °C) to remove contaminants. The whole bake out process normally takes several days. We wrapped the vacuum parts using heater tapes, which are powered by several variable AC transformers. Then we enclosed them in an oven built with fire bricks wrapped in aluminum foil. The key to a successful bake out is to carefully control the temperature change. Temperature gradients can apply significant stress and cause damage to the system. Caution must be taken when system is above 200 °C because some parts such as the window coatings, ion pump cables and titanium sublimation pump cables can not sustain higher temperatures. It is worth noting that we used silver-plated bolts on the knife-edge flanges to reduce the possibility of bolts seizing during the bake out process. Figs. 3.6 and 3.7 show the oven under construction and completed oven during the bake out process. The whole bake out process is tedious, but it is a necessary step to obtain an UHV system meeting the experimental requirements.

3.2.1 Pyramid MOT Vacuum Chamber

The pyramid MOT vacuum chamber was constructed from a six-port spherical square (Kimball Physics Inc. Model MCF450-SS20400-A). It consists of a thick-walled hollow spherical shell intersected with two 4.5″ CF (ConFlat) sealing surfaces, and four 2.75″ CF sealing surfaces. Traditional vacuum chambers used in cold atom

FIGURE 3.6: The oven under construction is prepared for the bake out. The variable AC transformers, heater tapes and thermocouple wires are shown in the picture.

FIGURE 3.7: The oven during the bake out process. The turbo pump and Residual Gas Analyzer (RGA) are mounted on the turbo pump station.

research labs are built by welding flanges to tubing segments of varying diameters and lengths. The resulting vacuum structures are often large and bulky. The vacuum chambers used in our lab use a unitary Multi-CF fitting design. Comparing to their welded counterparts, they are smaller, stiffer, cleaner, and better aligned.

One of the ports is equipped with a zero-length quartz optical window (4.5″ CF), which provides laser access to the pyramid MOT, and is obtained from Larson Electronics Glass, Model VQZ-250-F4. The port opposite to the optical window is connected to the differential pumping tube. The bottom port is sealed by a 2.75″ CF blank (HPS 100883000). A 20 L/s ion pump from Varian Inc. (Model VacIon Plus Starcell 20) is connected to the top port. One of the remaining two ports is connected to an all-metal valve (Varian 951-5027). When we bake out the vacuum chamber to get low pressure, we connect this valve to a turbo pump (BOC Edwards EXT 70H 24V). The last port is connected to another an all-metal valve (Varian 951-5027). Connected to this valve is a Rb breakseal ampoule (Alfa 10315 1g) and an ampoule breaker.

3.2.2 Differential Pumping Tube

The double-MOT system requires a big pressure difference between the two vacuum chambers where the two MOTs are formed. For quick loading of the pyramid MOT, the pyramid MOT vacuum chamber needs to have a pressure, dominated by Rb vapor, on the order of 10^{-8} torr. On the other hand, in order to satisfy the requirements of BEC experiments or few-atom quantum measurement experiments,

the science chamber should have a vacuum on the order of 10^{-11} torr. The three orders of vacuum pressure difference are achieved by the differential pumping tube [54] that connects the pyramid MOT vacuum chamber and the science chamber.

The differential pumping tube was made by drilling out a roughly cone-shaped structure in a stainless steel cylindrical tube (Fig. 3.8). This cone-shaped structure is about 6.3 inches long and consists of 12 cylinders with gradually changed diameters. The diameters increase in successive steps from an eighth of an inch at one end to one half of an inch at the other end, resulting in a tapered angle at about 3 degrees (similar to the design from [54]). The end with the smaller diameter is connected to the pyramid MOT chamber, and the end with the larger diameter is connected to the science vacuum chamber. This differential pumping tube has been calculated to have a conductance of ~ 0.05 L/s for Rb at room temperature. To calculate the conductance, we resort to the theory of gas flow through tubes and orifices [55]. The small conductance leads to about three orders of magnitude of pressure difference between the two chambers.

3.2.3 Science Vacuum Chamber

The science vacuum chamber was constructed from a six-port spherical cube (Kimball Physics Inc. Model MCF450-SC60000-C). It consists of a thick-walled hollow spherical shell intersected with six 4.5″ CF sealing surfaces.

Two of the six ports are equipped with optical windows. They are zero-length Pyrex viewports obtained from Larsen Electronics Glass, Model VP-250-F4. One of

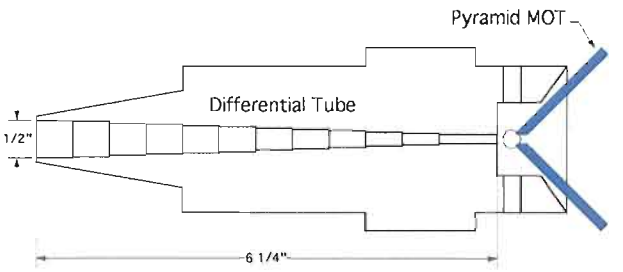

FIGURE 3.8: The differential pumping tube. The differential pumping tube has a low conductance of $\sim$ 0.05 L/s. It connects the pyramid MOT vacuum chamber and the science vacuum chamber, in which the magnitudes of pressure have 3 orders difference. Adapted from a mechanical drawing by D. Steck.

them serves just as a monitor port. The other one is used as an exit port to channel the dipole trap laser out of the vacuum chamber and dump it into a homemade beam dump. The bottom port is sealed by a 4.5″ CF blank (HPS 100885000), on which five non-evaporable getter pumps (SAES ST175/HI/16-30/300C) are mounted with electrical feedthroughs (Fig. 3.9). The getter pumps remove active gas from a vacuum via surface chemical adsorption and bulk diffusion. They pump hydrogen better than other kinds of vacuum pumps. Each getter pump gives a 45 L/s pumping rate for hydrogen. A four-way cross is connected to the top port. Connected to this four-way cross are a 75 L/s ion pump from Varian Inc. (Model VacIon Plus Starcell 75), a titanium sublimation pump (Duniway Stockroom TSP-275-003), and an all-metal valve (Varian 951-5027). This valve is used as a connection to the turbo pump during the bake-out process. The titanium sublimation pump was attached via an 90° elbow

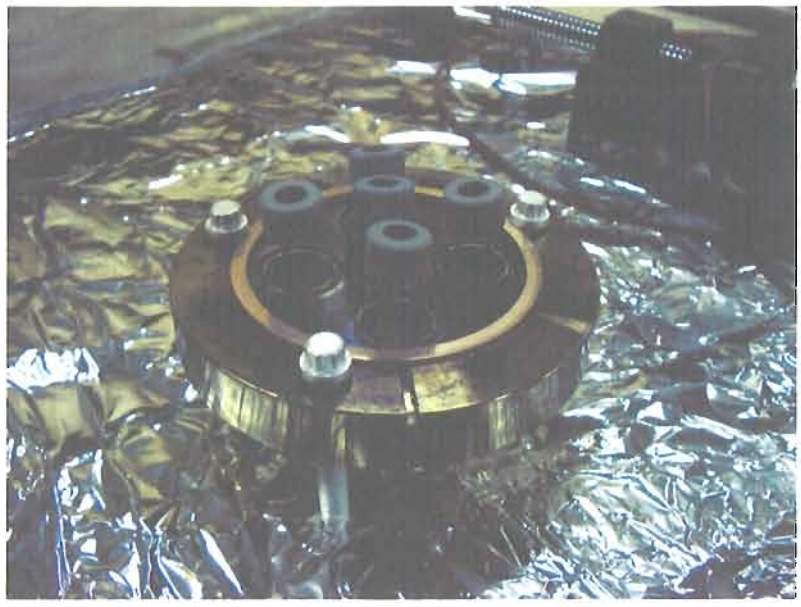

FIGURE 3.9: The getter pumps welded on the flange.

to avoid a direct line of sight from the filaments into any valve or pump. It will coat all surfaces in direct line with the filaments, and can cause valve sealing or pumping problems if not properly installed. The ion pump is turned on near the end of the bake-out process, and at the the same time the titanium sublimation pump and getter pumps are activated. As the workhorse to keep the vacuum, the ion pump is running continuously. A glass cell (Fig. 3.10) purchased from Hellma Cells, Inc. is attached to one of the two remaining ports, while the differential pumping tube is connected to the other one. The Hellma cell is made of Spectrosil 2000, a synthetic fused silica with high optical quality. The cell is rectangular with outer dimensions of 30 mm $\times$ 30 mm $\times$ 208 mm. The walls of the cell are 5 mm thick. The cell was made by optically contacting the individual walls together then increasing the temperature

until the pieces fused together. The open end of the cell is a Spectrosil flange, with 50 mm diameter and 10 mm thickness. The flange has a square center hole with side length 20 mm.

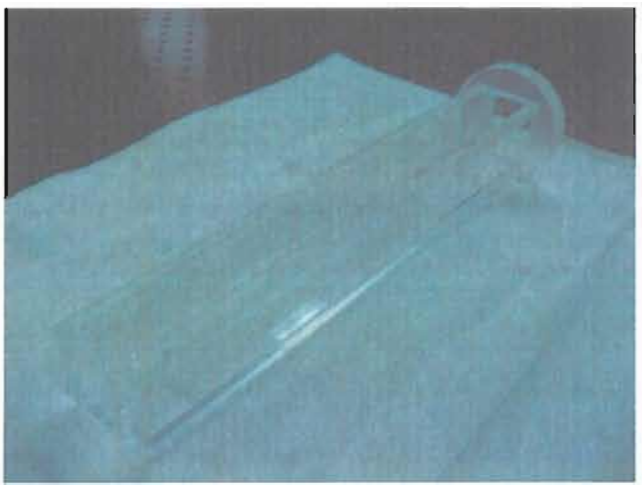

FIGURE 3.10: The Hellma cell.

The Hellma cell was mounted using a lead-alloy wire (Indium Corp, Indalloy 165) seal onto a $4.5'' - 2.75''$ zero-length CF reducer [56]. The zero-length CF reducer and a zero-length $2.75''$ CF flange were machined to have recesses to fit the Hellma cell flange (Fig. 3.11). Initially we used gold wire to seal the Hellma cell, but we cracked the Hellma cell, which indicates that the torque applied on the $1/4 - 28$ mounting bolts (120 in-lb) was too much. (Note that the gold wire worked on a quartz window.) Later we used the lead-alloy wire instead. Since lead is softer than gold, much less torque (30 in-lb) is required. It passed a helium leak test and worked well.

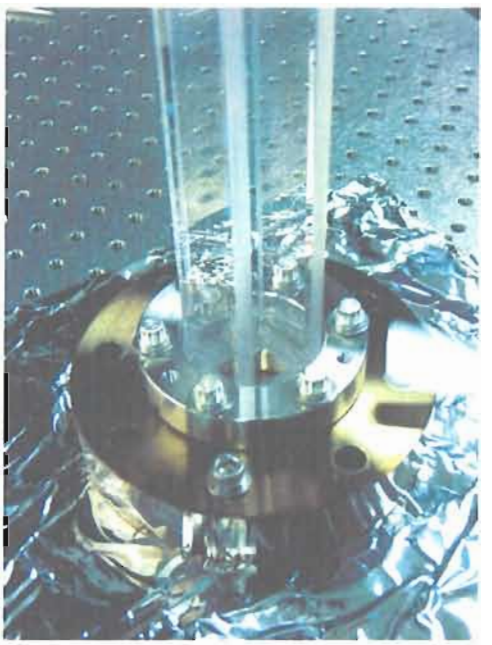

FIGURE 3.11: The Hellma cell is mounted on the zero-length CF reducer.

3.3 Laser System

The laser system in our experiment is very extensive. In general, the lasers can be grouped into two different categories. The first is mainly used in the MOT (magneto-optic trap) operation and the "one-way optical barrier" experiment. They cool and trap atoms, optically pump atoms, image atoms, and provide the one-way optical barrier. Determined by the task they perform, these lasers are all tuned near Rb atomic resonances. The second is to create the dipole trap, which is far off all atomic resonances. The optics layout is shown in Fig. 3.12. Note that the dipole-trap laser is not shown. The absorption imaging beam is derived from the six-beam MOT slave

laser. The repumping barrier beam used for the one-way barrier experiment is split off the repump laser. They are not shown in the figure either.

The laser frequencies and relevant energy levels used in our experiment are displayed in Fig. 3.13.

3.3.1 Near Resonant Lasers

The operation of a Rb MOT needs two lasers with different frequencies. In our experiment, the cooling and trapping is done by one laser that is tuned slightly to the low-frequency side of the $5S_{1/2}$, $F = 2 \rightarrow 5P_{3/2}$, $F' = 3$ transition of ^{87}Rb. F and F' denote the total atomic angular momentum including the nuclear spin. Unfortunately, about one excitation out of 1000 will cause the atoms to decay to the $F = 1$ state instead of the $F = 2$ state. The atoms in the $F = 1$ state are not near resonance with the cooling and trapping laser. We use another laser (called the "repump laser") to excite the atoms from $5S_{1/2}$, $F = 1$ to $5P_{3/2}$, $F' = 2$ state, from which the atoms can decay back to $5S_{1/2}$, $F = 2$ state, where they will again be excited by the cooling and trapping laser.

In addition to cooling and trapping the atoms, a near-resonant laser is also used in the one-way barrier experiment to create the barrier. Due to the variety of frequencies required as well as the amount of laser power necessary, five diode lasers are employed. One of the diodes is the master laser that produces "seed light" for two slave lasers for the two MOTs in our double-MOT system. The other two diode lasers produce the light for repump and barrier purposes.

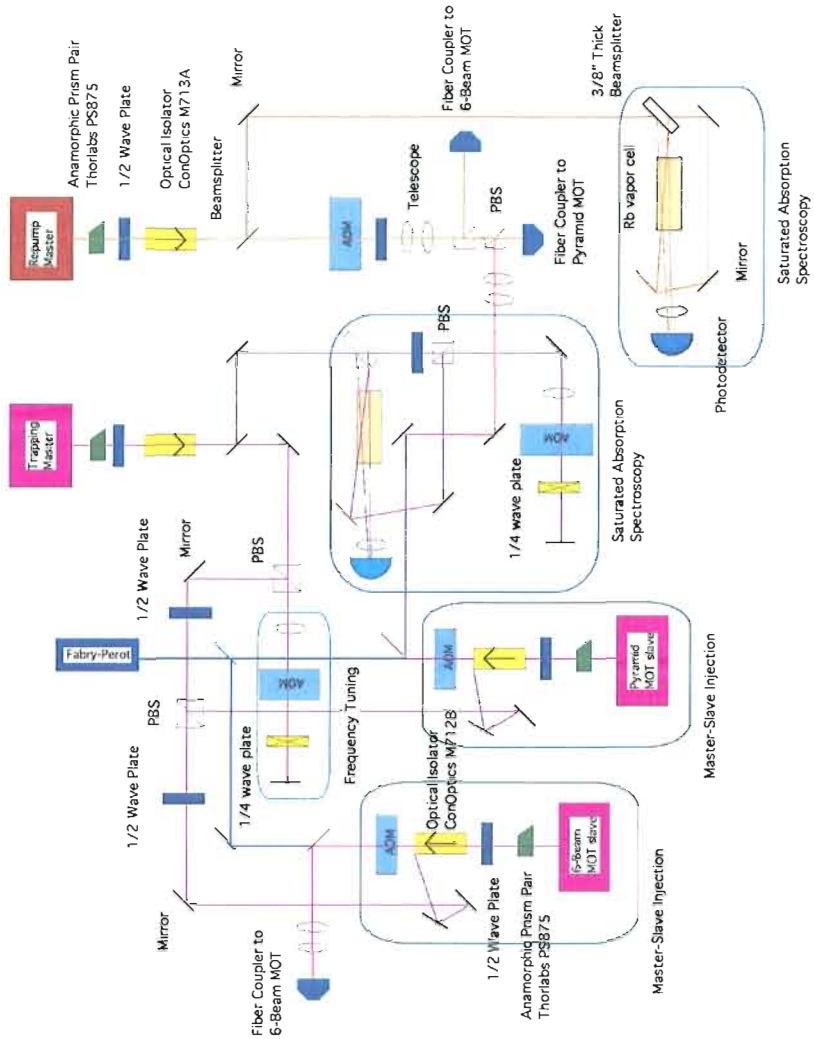

FIGURE 3.12: The schematic drawing of the main optics layout. It includes the MOT master laser, repump laser, pyramid MOT slave laser, six-beam MOT slave laser, and their frequency-stabilization optics.

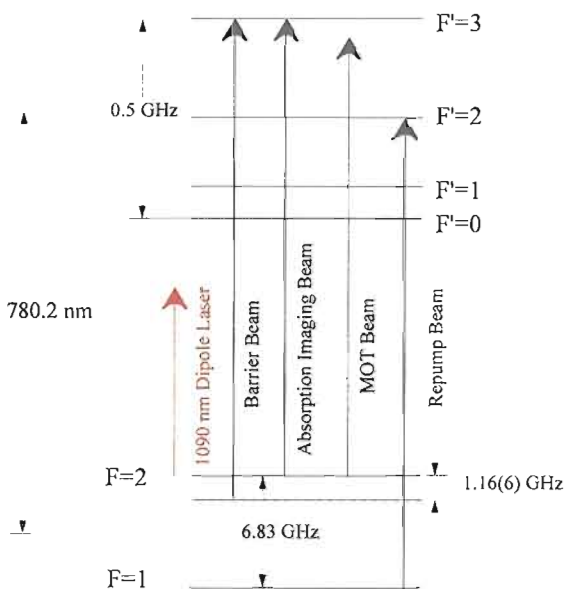

FIGURE 3.13: The multitude of laser frequencies and related energy levels used in the experiment. Note that the figure is not to scale.

3.3.1.1 MOT Master Laser

The MOT master laser produces the "seed light" near the $5S_{1/2}$, $F = 2 \rightarrow 5P_{3/2}$, $F' = 3$ transition of ^{87}Rb.

The experiment requires precise control of laser frequency. The laser linewidth should be narrower than the natural linewidth of the atomic transition. The laser output from an "off the shelf" laser diode is typically some tens of MHz wide and the laser diode can be continuously tuned only over certain limited region. The laser diode characteristics can be greatly improved by using external-cavity optical feedback.

There are two excellent papers that give general background of diode lasers and detailed instructions on how to build external cavity diode lasers: "Using diode lasers for atomic physics" [57] and "A narrow-band tunable diode laser system with grating feedback and a saturated absorption spectrometer for Cs and Rb" [58].

Construction of External Cavity Diode Lasers

The external cavity diode laser has three basic components, a commercial diode laser, a collimating lens, and a diffraction grating. The diode used is a GH0781JA2C laser diode manufactured by Sharp Microelectronics and purchased from Digi-Key. The typical lasing wavelength of the diode is 784 nm. The maximum output optical power is 120 mW.

The laser was modified by Daniel Steck from the original design of Buce Klappauf [59], Daniel Steck [60] and Windell Oskay [61], in that the angle of the grating

was adjusted to work at 780 nm. It was machined by the UO machine shop and assembled in our lab. The material used for laser mounting block, grating mounting block, and laser base plates is 954 aluminum bronze. This material has good thermal conductivity, which is good for temperature stabilization. It also has high strength and resistance to fatigue, which is required for the adjustment of the laser system. The base plate of the housing is made of aluminum. The MOT master laser is shown in Fig. 3.14.

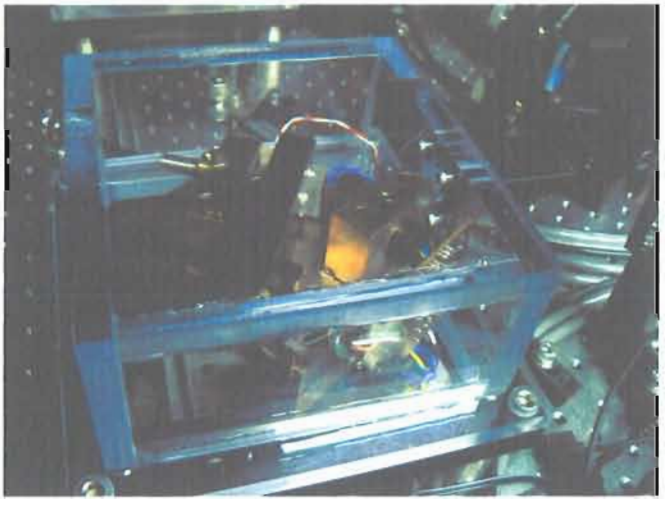

FIGURE 3.14: The MOT master laser. The photograph shows the housing, grating and laser protection board.

The external cavity is formed by the reflective back surface of the diode, and the diffraction grating is used as a wavelength-selective output coupler. In the Littrow configuration [62] (see Fig. 3.15) adopted in our design, the first-order beam diffracted from the grating reflects back into the cavity and provides optical feedback. Semiconductor diodes are very sensitive to feedback due to their wide gain bandwidth.

The back-reflected beam injection can lock the diodes. The zero-order reflection from the grating forms the output beam. The emission wavelength can be tuned by rotating the diffraction grating. A disadvantage of the Littrow configuration is that rotating the diffraction grating also changes the direction of output beam. In practice, the output power from our MOT master laser is about 40 mW.

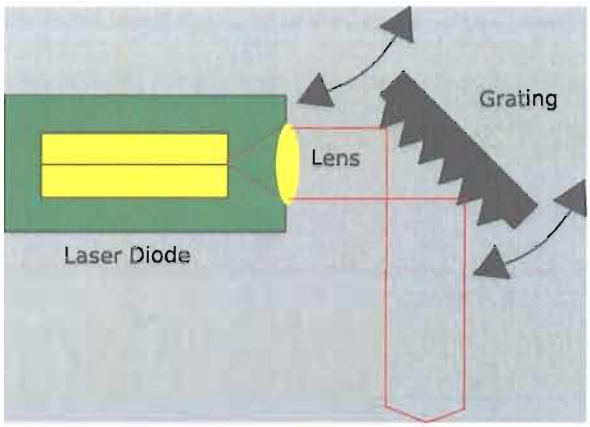

FIGURE 3.15: The Littrow configuration.

The incident angle between the grating and the laser beam has to satisfy the Littrow condition

$$m\lambda = 2d\sin\alpha \tag{3.1}$$

where m is the diffraction order, d is the grating spacing, α is the grating angle, and λ is the laser wavelength near 780 nm. The grating used in the MOT master laser was procured from Edmund Scientific (part number E43005), which has a ruling of 1200 grooves/mm, or a spacing of $d = 0.833$ μm. The measured grating efficiency is about 70%. The grating angle α is about 27.9° for a 780 nm output laser. The

grating we initially purchased was $1'' \times 1'' \times 3/8''$. In order to fit in the grating mount, we cut it in 4 pieces that are $1/2'' \times 1/2'' \times 3/8''$. The cutting can be safely done as follows [57]. Apply a coating of acetate fingernail polish to the ruled surface of the grating using a soft hair brush. Avoid any physical contact of the brush with the grating. After the coating is dry, wax the back of the grating to a block of bakelite to support the grating while it is sawed. Mark the coated surface of the grating into pieces of the desired size. Mount with the supporting block and saw the grating with a diamond saw. Then remove the coating by submerging the grating segments in a small beaker of methanol and placing the beaker in an ultrasonic cleaner. Take the gratings out using tweezers with great care, refill the beaker with fresh methanol, and repeat several times until the gratings appear completely clean. Later we purchased gratings with the dimension of $1/2'' \times 1/2'' \times 3/8''$ directly from Edmund Scientific. So we saved the work of cutting for other diode lasers we made. In order to alter the cavity length with the electrical control, we inserted a piezoelectric stack (Noliac SCMA/S2/A/5/10/60/9/1500) between the grating mount adjustment screw and the movable arm of the mount. The maximum voltage that can be applied on the piezoelectric stack is 60 V, and the displacement is 0.17 μm/V. Given the piezoelectric stack and our 15 V electronics, the expected frequency tuning range is $\sim$ 30 GHz.

Single-Mode Operation of External Cavity Diode Laser

The construction of the grating-stabilized, external-cavity diode laser is relatively

simple. To achieve single-mode operation of the diode laser on one of the ^{87}Rb spectral lines can be time-consuming and technically difficult. Details of the procedures used to align the laser are documented here. The starting point is to collimate the diode laser. This is accomplished using a Thorlabs collimation tube, model LT230P-B. The collimation tube has a 4.5 mm focal length collimation lens and a numerical aperture of 0.55. We aim the laser beam at a distant wall ($>$ 5m). Then we monitor the spot using an IR viewer while using a spanner wrench to adjust the distance between the collimation lens and laser diode continually until the spot on the wall is minimized. After the laser diode is collimated, we set the polarization direction to be vertical. This is done using a polarizing cube beam splitter (PCBS) and a power meter. When the power of the laser beam transmitted through PCBS is minimized, the output beam polarization is vertical. Diode lasers have an inherently elliptical beam shape due to the geometry of the diode junction. We use an anamorphic prism pair (Thorlabs PS875 2.0 X) to transform the elliptical beam emerging from the collimation lens into a nearly circular beam. The anamorphic prism pair does this by expanding the beam in only one dimension while the other dimension remains unchanged. External-cavity diode lasers are very sensitive to light back-reflected into them. Isolation of at least 30 dB is typically required for external cavity lengths of 1 cm to 10 cm [62]. We use an optical isolator (Conoptics M713A) to eliminate the back reflection. The optical isolator consists of a Faraday rotator and two beamsplitting polarizers which are rotated 45° relative to each other. After the light propagates through the first

polarizer and the Faraday rotator, it is rotated by 45°, i.e. the same direction as the second polarizer. The returning light from any reflecting surfaces undergoes an additional 45° rotation in its backward pass. It is now polarized orthogonal to the forward beam and is rejected by the first polarizer. The isolation we measured is about 40 dB.

After the laser diode is collimated, the beam shape is corrected, and optical isolation is ensured, the output power and threshold characteristics are measured. This is accomplished by modulating the laser current using a triangle wave from a function generator and monitoring the output power. The modulation signal (about 10 Hz) is sent to channel X of an oscilloscope that is set to X-Y mode, and the output from power meter is sent to channel Y. The turning point on the scope shows the laser threshold.

Now it is time to adjust the grating to self-inject the laser. We lower the diode injection current to just below the threshold level. Then we modulate the diode current and observe the power output on an oscilloscope. A shallow slope is shown on the oscilloscope until the threshold current is reached, at which point the slope shows a sharp increase. The trace will change shape according to the vertical angle of the grating. When the grating is properly aligned, the threshold current will drop. We can observe the turning point moving to a lower current value, and the trace becomes sharper at the turning point. If current modulation is not available, the grating can be aligned by observing the threshold current and output power by eye.

The output beam should be significantly brighter at the exact vertical position that optimizes feedback into the diode, and the threshold current will be lower than the value recorded earlier. When the grating alignment is made, it is important to make sure the achieved threshold is not a local minimum, but is the global minimum value. If there is more than one vertical setting of the grating to enhance the laser output near threshold, or the output beam projected on a distant surface consists of more than a single collimated spot, the fault may be the imperfections such as chips, dirt, or scratches on the grating, laser window, or lens surfaces.

Next we shine the laser through a Rb absorption vapor cell (Triad Tech TT-RB-75-V-P). The frequency of the laser is swept by adjusting the horizontal angle of the grating. Normally, when we make small adjustments of the horizontal grating alignment with the PZT being ramped, we can easily see the fluorescence. If no fluorescence is apparent at any grating angle within the tuning range, then most likely there is tuning discontinuity that encompasses the absorption line wavelength. If it is difficult to find fluorescence by tilting the grating, it is necessary to operate the laser at a different temperature and/or current. The current should be changed by several mA and the procedure repeated. If this still does not work, the temperature should be changed up or down. After the horizontal angle of the grating has been set to approximately the correct wavelength, the vertical alignment should be checked using the threshold-current technique. Sometimes when one nears the end of grating tuning range, the laser output will hop back and forth or share power between two

very different frequencies. One is the fixed, "free-running" frequency at which the laser will operate if there is little or no feedback from the grating, and the other is the angle-dependent frequency set by the grating. The grating is appropriately aligned when the vapor cell fluoresces and the laser spectrum from the Fabry-Perot cavity is single mode. If the vapor cell fluoresces but the laser is multi-mode, an iterative process of tuning the laser current and adjusting the grating is necessary. At last, we adjust the temperature of the diode to optimize the operating current. Normally we set the operating current near 100 mA (for safety of the laser diodes), which is a little below the nominal operating current listed on the data sheet (120 mA). Once the whole procedure is finished, it usually does not need to be undertaken again until the diode is replaced. The operation of a diode laser predominantly depends on the particular diode. Some diodes are easy to set up, but it is difficult to get some other diodes working well.

To determine the laser wavelength precisely, we need to perform Doppler-free, saturated-absorption spectroscopy experiments. Such experiments provide the simplest way to determine the short- and long-term frequency stability and tuning behavior of the laser frequency. Also, they are essential to actively stabilize the laser output frequency. The apparatus for saturated-absorption spectroscopy is shown in Fig. 3.16. There are three similar sets of saturated-absorption spectroscopy systems for the MOT laser, the repump laser and the one-way barrier laser. Here, we describe the common elements used for all lasers. We pick off a small amount of the master-

laser output light for the spectroscopy. A 3/8″ thick beamsplitter splits this part of the master-laser output beam into three parts, two less intense beams and a more intense beam (pump beam, about 90% beam power). The two weak beams propagate through the rubidium vapor cell. Then they are separately detected by two photodiodes. The two photodiodes and a differential photodetector circuit, which subtracts the two photodiode signals, are mounted in a small box to record the spectral lines. The pump beam passes through the rubidium vapor cell in the opposite direction of the two weak beams and overlaps one of them after being reflected by three mirrors. We call the overlapping weak beam the "probe beam" and the other one the "reference beam." If we block the pump beam and the probe beam, the signal from the reference beam will show a Doppler-broadened absorption spectrum. Around 780 nm, there are four Doppler-broadened rubidium absorption lines, two outer lines for the 28% abundant ^{87}Rb and two inner lines for the 72% abundant ^{85}Rb. If the reference beam is blocked, the signal from the probe beam will show "dips" in the Doppler-broadened absorption lines. If both weak beams are unblocked, the Doppler-broadened line cancels in the subtraction, and the dips reflecting the hyperfine structure remain. Fig. 3.17 shows the saturated transmission spectrum of Rb.

Since saturated-absorption spectroscopy is very important to our experiment, we discuss the physics briefly here. The pump beam changes the populations of atomic states and the probe beam detects these changes. Because of the Doppler shift, only atoms with a particular velocity v will be in resonance with the pump beam and

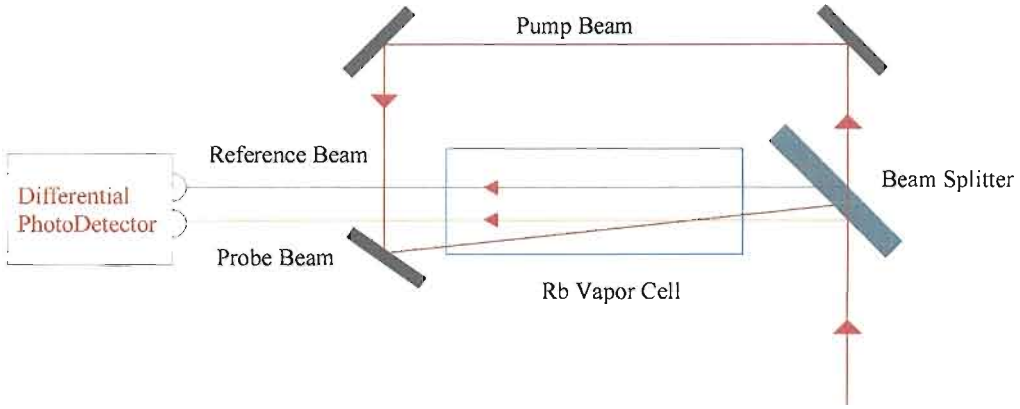

FIGURE 3.16: Optical setup for saturated absorption spectroscopy. A small amount of laser light is sent through a beamsplitter to produce a strong pump beam and two weak beams, one being the reference beam and the other the probe beam. Both weak beams pass through a Rb vapor cell and are sent to two photodiodes where signals are subtracted. The pump beam is sent to the Rb vapor cell counter-propagating with the probe beam.

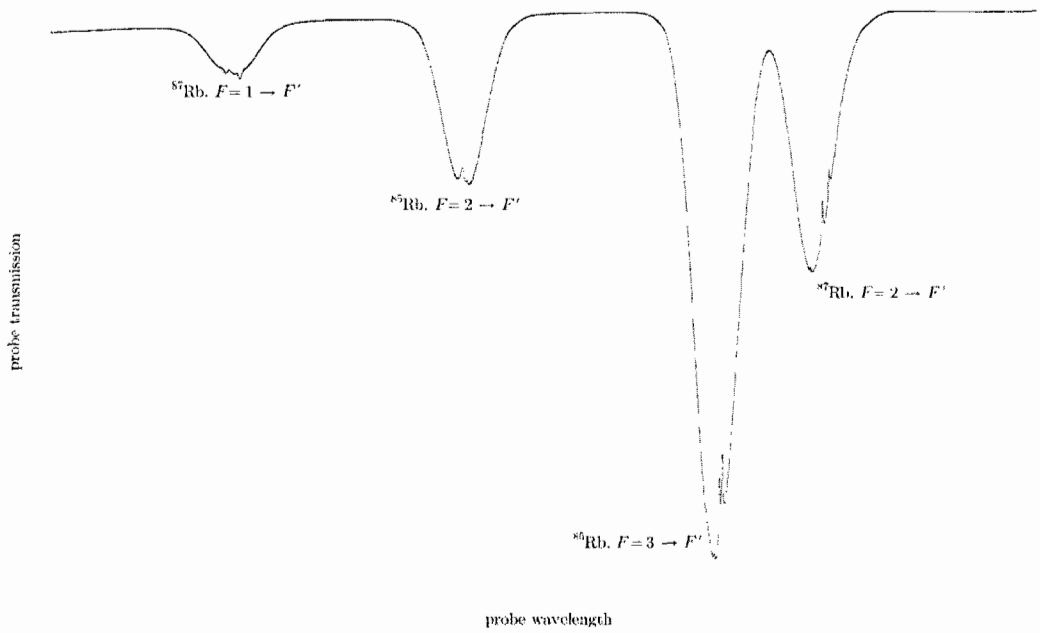

FIGURE 3.17: The saturated transmission spectrum of Rb (made by D. Steck).

excited. This velocity-dependent excitation process changes the populations in two ways. One way is called "hyperfine-pumping" and the other "saturation." Hyperfine-pumping is the larger of the two effects, and refers to the optical pumping between the hyperfine levels of the $5^2S_{1/2}$ states (see Fig. 3.13). Suppose the laser can excite an atom in the $F = 1$ ground state to the $F' = 1$ excited state. The ΔF selection rule indicates that this excited state can decay back to either the $F = 1$ or $F = 2$ ground state with roughly comparable probabilities. When the atom decays back to the $F = 1$ state, it will be excited again and the process repeats. Thus after a short time interval, most of the atoms will be left in the $F = 2$ state. If the laser intensity is sufficient to excite the atoms on microsecond time scales, it will cause a significant

change in the population of the $F = 1$ and $F = 2$ levels. Similar hyperfine-pumping will occur for any excitations where the excited state can decay back into a ground state that is different from the initial ground state. The other process by which the laser excitation changes the ground-state population is "saturation." When an atom is excited to an F' level it will spend about 28 ns in this level before it decays back to the ground state. If the pump-beam intensity is low, the atom will stay in the ground state for a much longer time before it is re-excited. So, on average, most atoms are in the ground state. But if the pump-beam intensity is high enough, it will excite the atom very rapidly. In the high-intensity limit, half the population is in the ground state and half is in the excited state. Saturation will occur on transitions that have hyperfine-pumping as well as on transitions that do not. It is generally a smaller effect than hyperfine-pumping. Hyperfine-pumping will occur at much lower intensities than saturation. The intensities used in saturated-absorption spectroscopy are low enough that the hyperfine-pumping effect dominates the saturation effect. This can explain why the $F = 2 \rightarrow F' = 3$ and $F = 1 \rightarrow F' = 0$ spectral lines (see Fig. 3.13) are much weaker than the other spectral lines in the saturated absorption signal. These two transitions are "cycling" transitions, in the sense that the atoms decay from the excited state back to the same ground state, and thus the hyperfine-pumping effect is weak. As one increases the intensity these absorption peaks will become larger relative to other peaks when the saturation effect becomes important. Atoms with the speed $v = 0$ in the region where the probe and pump beams overlap can absorb

light from both the beams. For example, for the $F = 1 \rightarrow F' = 1$ transition (see Fig. 3.13), the pump beam depletes the population of the $F = 1$ state, so the probe beam will pass through the vapor cell with reduced absorption. The reference beam will not experience absorption reduction; hence, subtraction of the two signals gives a signal without Doppler broadening. For $v \neq 0$, the three beams will interact with three different groups of atoms. There are some "crossover" spectral lines shown on the saturated absorption signal. The crossover dips appear midway between any two transitions that have the same lower level and two different excited levels. When the laser is tuned to the frequency midway between two transitions, atoms with a particular nonzero velocity can simultaneously be resonant with both the pump and probe beams and thus have nonlinear absorption. The absorption here is saturated not in stationary atoms, but rather in atoms moving such that two beams are resonant with the two different transitions in the rest frame of the atoms. The crossover dips are often stronger than the normal resonances, since the nonlinear spectral signal arises from depletion instead of saturation.

Laser Frequency Control and Stabilization

All of our near-resonant diode lasers are locked to atomic transitions in ^{87}Rb or ^{85}Rb using saturated-absorption spectroscopy. The use of a Doppler-free saturated absorption signal as a frequency reference has become a standard technique in maintaining laser frequency stability [58].

Traditional methods for frequency stabilization use feedback to minimize the laser frequency offset from an absolute reference, such as atomic and molecular absorption lines, or a Fabry-Perot interferometer. We first review basic concepts of frequency stabilization before we present the details of our frequency stabilization scheme and setup.

The diode laser frequency is determined by its injection current, temperature and the grating angle. In order to obtain a stable laser frequency, one must stabilize the diode's temperature and injection current. Our diode lasers use the Littrow configuration, where the output beam reflects off the grating, and the first-order diffraction is sent back into the laser diode. The effect of optical feedback from the grating is a spectrally narrowed laser output, possibly peaked at a frequency different from the central frequency of the free-running diode laser. The optical feedback from the grating narrows the laser frequency bandwidth from 50 MHz to about 1 MHz. But over time, the diode-laser central frequency will drift due to fluctuations in temperature and injection current, and also mechanical noise. To reduce this drift, we can lock the laser to an external frequency reference. The general idea is to generate a frequency error signal that passes through zero at the locking frequency. Fig. 3.18 illustrates the fundamental idea for stabilizing the laser frequency. Part of the laser light is compared with a frequency reference, and the error signal is fed back to the diode laser. There are many frequency-stabilization schemes based on

different frequency references. The most common techniques make use of Fabry-Perot interferometers or atomic transition lines.

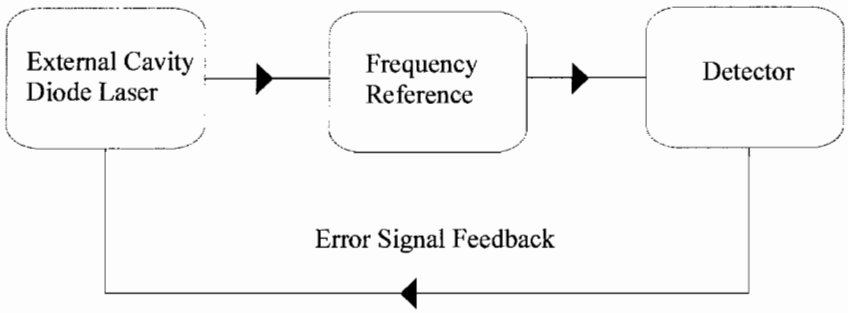

FIGURE 3.18: The basic frequency stabilization scheme of diode lasers.

We use saturated-absorption spectroscopy for a frequency reference to stabilize the diode lasers. The basic idea of this method is to generate sub-Doppler spectral lines, which are used as a reference to stabilize the laser. A non-zero error signal alone is insufficient to determine whether the laser frequency should be increased or decreased to correct the error. So a servo can only work in a region where there is a slope to use as feedback. A simple solution is to lock the laser the side of a spectral line. But the side lock is sensitive to beam alignment, beam intensity, and broadening effects, which would cause the locking point to change. To overcome these drawbacks, we lock each laser to the peak of an atomic transition line instead of the side of it. If the laser frequency has been adjusted to equal the peak frequency, a drift towards higher or lower frequency will causes an error signal of the same sign. In

order to lock to the peak of an absorptive line and get a slope around the peak area, we generate a "dispersive" signal (the derivative of the saturated absorption signal) by either modulating the laser current or the radio frequency driving an acousto-optic modulator (AOM). In our MOT-laser frequency-stabilization setup, we use an AOM to modulate the frequency of the light entering the saturated absorption cell. The signal from the saturated-absorption setup is fed to a homemade lock-in detector, which generates the derivative of the saturated absorption signal. This derivative changes sign at the center of the spectral peak, making it an ideal error signal. In our repump laser frequency-stabilization setup, we directly modulate the laser current for its simplicity. It has the disadvantage that the main repump beam frequency and intensity are modulated, but since the MOT operation is relatively insensitive to the repump characteristics, it is not a big problem.

We already described the common part of the saturated-absorption setups for the MOT master laser, repump laser, and barrier laser. The difference between the setup of the MOT laser and the setups of the repump and barrier lasers is in the different methods used to modulate the laser frequency. A layout of the saturated-absorption setup for the MOT laser frequency stabilization is shown in Fig. 3.19. A small portion of the MOT master laser is picked off from a beamsplitter and fed into the saturated-absorption spectroscopy setup. This beam propagates through a $3/8''$ thick beamsplitter. The reflections from the two surfaces of the beamsplitter produce two weak beams ($\sim 100\ \mu$W), which propagate through the Rb vapor cell from right

to left. The stronger transmitted beam goes through a polarization beamsplitter cube (PBSC) which directs the beam to an acousto-optic modulator (AOM). The AOM (IntraAction ATM-1451A2) is driven by a frequency-modulated signal with a center frequency of 145 MHz that switches between 143 MHz and 147 MHz at a frequency of 200 kHz. The first order of the AOM goes through a quarter-wave plate and is then retro-reflected on a curved mirror. The beam then retraces its path back to the AOM, where it is diffracted again. This double-pass configuration reduces movement of the output beam when its frequency is modulated. The first order goes back to the PBSC and this time it is reflected due to the orthogonal polarization from the two passes through the quarter-wave plate. Upon reflection, the beam (pump beam) enters the Rb vapor cell from left to right and overlaps with one of the two beams reflected from the 3/8″ thick beamsplitter. We again call this beam the "probe beam" and the other one which is reflected from the 3/8″ thick beamsplitter the "reference beam." The probe beam overlaps with the pump beam which is 290 MHz higher in frequency on average due to the AOM. So in the Rb vapor cell, these two beams interact with a velocity class of atoms corresponding to a frequency shift of 145 MHz. The probe beam and reference beam propagate through the rubidium vapor cell and are separately detected by two photodiodes. Differential photodetector circuitry subtracts the signals from two photodiodes, and the subtracted signal is sent to a homemade lock-in amplifier. The lock-in amplifier also receives the same signal used to modulated the frequency of the double-passed AOM. The lock-in amplifier uses

these to generate a signal that is proportional to the derivative of the saturated-absorption signal. This dispersive signal is used to lock to a particular transition.

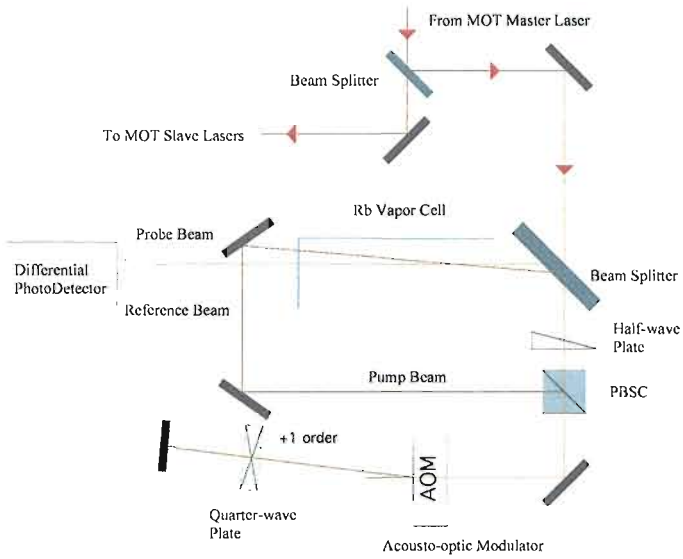

FIGURE 3.19: The optical layout for saturated-absorption spectroscopy used for the MOT master laser frequency stabilization. The signal from a differential photodetector is sent to a lock-in amplifier, which receives the same reference signal used to modulate the AOM.

The MOT master laser is locked to the $F = 2 \rightarrow F' = 2/3$ crossover transition, which is the strongest line in the spectrum. The AOM in the saturated-absorption setup shifts the beam up by 145 MHz, so the output beam of the laser is 145 MHz red of transition to which it is locked. The $F = 2 \rightarrow F' = 2/3$ crossover transition is 133 MHz red of the $F = 2 \rightarrow F' = 3$ cycling transition, so the output beam from the MOT master laser is 278 MHz red of the cycling transition.

We use a double-passed acousto-optic deflector (AOD) to tune the MOT master laser frequency. The deflector (IntraAction ATD-801A2) has a center frequency of 80 MHz and a 3 dB bandwidth of 40 MHz. The frequency of the MOT master laser can be raised by 120 MHz to 200 MHz using the first order in the double-pass configuration, so the MOT master laser will have a detuning of 78 MHz to 158 MHz red of the cycling transition after the double-passed AOD. We then inject this MOT master laser beam into a slave laser. The slave laser has the same spectral properties as those of the MOT master laser. The output beam from the slave laser passes through an 80 MHz AOM, and the first order is used for the experiment. This 80 MHz AOM (IntraAction ATM-801A2) functions as both a fast shutter and a frequency shifter that shifts the laser frequency from about 2 MHz blue to 78 MHz red of the $F = 2 \rightarrow F' = 3$ transition. This is a sufficient range of detunings for successful operation of the experiment.

3.3.1.2 Slave Lasers

The output power from the MOT master laser is about 40 mW. Between the laser and the MOT, there are many optical component that reduce the power even more. Remember that we use additional "slave" lasers to compensate for the power loss and provide the required power for the experiment. Our experimental setup consists of a double-MOT system: a pyramid MOT as a slow atom source and a six-beam MOT with which the experiments are conducted. Not surprisingly, we have two slave lasers

used for our experiment. One is for the first MOT (pyramid MOT), and the other one is for the second MOT (six-beam MOT). These slave lasers (see Fig. 3.20) are injection-locked to the MOT master laser.

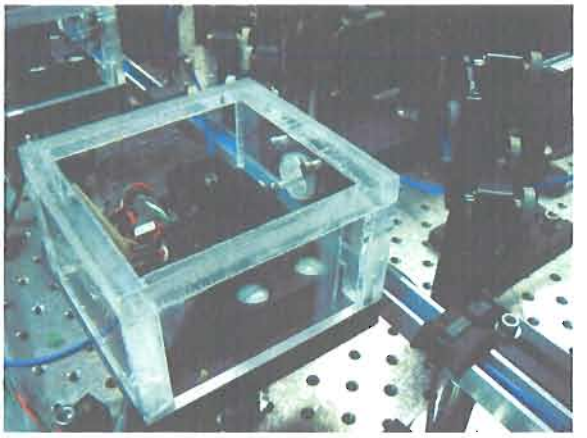

FIGURE 3.20: A slave laser. It shows the laser diode holder, the electrical connections and the housing with an optical window at Brewster's angle.

The slave lasers are free running-laser diodes. We use the same laser diodes as those for the MOT master laser. Thorlabs collimation tubes (LT230P-B) are used to collimate each of the two laser diodes. The collimation tube resides in a $2.25'' \times 1.372'' \times 1.5''$ aluminum mounting block, which is on the top of a Melcor thermoelectric cooler (TEC), model CP1.0-127-05L. The TEC is mounted between the laser diode mounting block and a $3.5'' \times 3.25'' \times 0.5''$ aluminum base plate. The hot side of the TEC is in contact with the base plate, while the cold side of TEC is in contact with the laser-diode mounting block. A 50 kΩ glass thermistor (Fenwall Electronics, part number 121) is used with the TEC to regulate the laser diode temperature. A temperature sensor IC, model AD590JH, is used to read out the laser-diode temperature. A

Wavelength Electronics module, model WTC 3243, provides the temperature-control electronics. There are two different connectors related to the slave laser: a 9 pin D-subminiature connector (Amphenol 17SD-E9P) for the temperature controller, and a 5 pin Redel gray plastic connector from Lemo USA Inc. for the current controller. The cover of the slave laser is made of Lucite for thermal isolation. The output window is made from a $1'' \times 3'' \times 1$ mm microscope slide mounted at the Brewster angle.

In order to get the same spectral properties of the MOT master laser, the slave lasers are injection-locked [63]. In injection-locking, a weak signal at a frequency within a narrow locking range around the free-running frequency of a "slave" oscillator is injected into the slave's resonant circuit. The slave oscillator can then phase-synchronize to the input.

We send a small portion of light from the MOT master laser into the slave lasers. If the spatial profiles are sufficiently matched, the slave lasers will be controlled by the seeds from MOT master laser and have identical spectral properties with full power output (typically 100 mW). The injection locking is implemented using an optical isolator. The injected light from MOT master laser is set to have a polarization that is orthogonal to the slave laser and sent into the rejection port of the optical isolator. The optical isolator rotates the polarization the same direction irrespective of the propagation direction, so the injected beam exits the optical isolator with the same polarization as the slave laser. We make an effort to align the injected beam to be co-

linear with the slave-laser output beam and to match the spatial profile of the injection beam to that of the slave laser. The co-linear alignment is accomplished by adjusting two mirrors prior to the optical isolator. There are special techniques to tune the lasers for injection locking. First, we adjust the current and temperature of the free running diode lasers and make sure the output beam fluoresces when going through the Rb vapor cell. Second, we align the injected beam to be counter-propagating with the slave-laser output beam. Then we use a Fabry-Perot cavity to analyze the slave output. We observe the slave-laser spectrum while sweeping the frequency of injected MOT master laser beam. Normally we will see a peak corresponding to the free-running slave laser and a small moving peak corresponding to the portion of the slave laser injection-locked to the frequency-swept MOT master laser. Then we do the following things to optimize the injection locked peak. First, we adjust the slave laser current to maximize the injection-locked peak. Next, we adjust the alignment of the injection beam to maximize the injection-locked peak. After the current and alignment are optimized, we try to minimize the injection-beam power required to lock the slave laser. This process is done by decreasing the injection beam power until the slave is not completely locked. Then the current and beam alignment are adjusted to relock the slave. The whole procedure is iterated until the lock is optimized.

Pyramid MOT Slave Laser

The layout of the pyramid-MOT slave laser is shown in Fig. 3.21. It goes through

an anamorphic prism pair (Thorlabs PS875 2.0 X) to correct the beam shape after exiting the laser housing. Then it passes through an optical isolator (ConOptics M712B) to prevent potential back-reflections. This optical isolator also functions as the optical port to inject the slave laser with a small amount of the MOT master laser light. Then the laser transmits through an 80 MHz AOM (IntraAction ATM-801A2) and the first-order beam passes through a homemade mechanical shutter. It is combined with part of the repump laser output beam at a PBSC, then coupled into a polarization-maintaining fiber and sent to the pyramid MOT. The zero-order beam from the AOM is sent to a homemade Fabry-Perot cavity to monitor the laser spectrum.

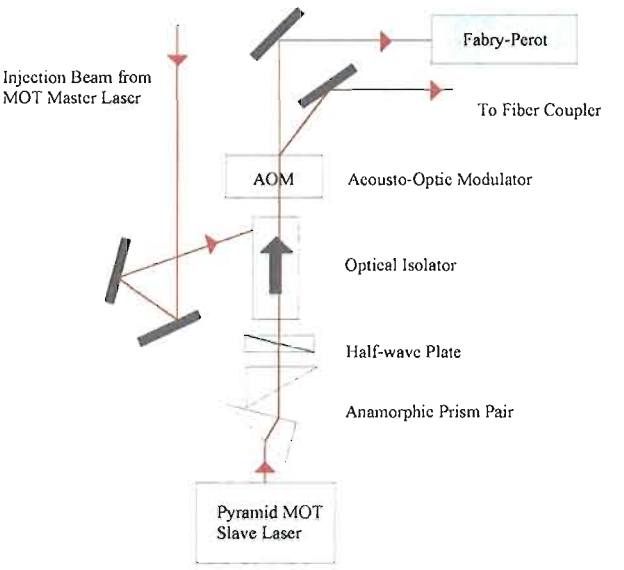

FIGURE 3.21: The optical layout of pyramid MOT slave laser.

Six-beam MOT Slave Laser

Most of the optical layout of the six-beam MOT slave laser is the same as that of the pyramid MOT slave laser (see Fig. 3.21). The first-order beam from another 80 MHz AOM is coupled into a polarization-maintaining fiber which connects to an input port of a fiber splitter. The fiber splitter (Canadian Instrumentation and Research Ltd., Model 5929-1) has two input ports and six output ports, which provide the light beams for the six-beam MOT. (The other input port is for the repump laser.) The zero-order beam from the AOM is split by a microscope slide. The transmitted beam is sent through an 80 MHz AOM and a homemade mechanical shutter adapted from the design of Singer [64] (see Fig. 3.22). After this mechanical shutter, the beam is coupled into a polarization-maintaining fiber and used for absorption imaging. Since the extinction of the AOM is not perfect, the mechanical shutter is used to guarantee there is no leakage light. The AOM is a fast and imperfect shutter, while the slow mechanical shutter gives perfect extinction. This mechanical shutter is made of a speaker with an aluminum flag attached to the coil of an inexpensive speaker. In order to get high-quality absorption imaging, part of the absorption-imaging beam is sent to a pulse stabilization circuit, which uses controls the pulse length to correct for intensity fluctuations. It integrates the pulse, and shuts it off when the integration reaches a certain value.

We also built another version of mechanical shutter, as shown in Fig. 3.23. It is a relay with an extended arm [65]. The arm is made of a small metal tube, at the

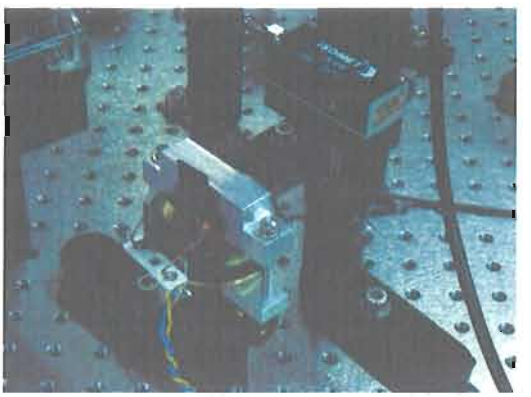

FIGURE 3.22: The mechanical shutter used for the absorption imaging beam. A speaker coil is used to move an aluminum flag to block the laser.

end of which is a flag made of a razor blade painted black. The flag will block the beam if the relay coil is driven by a current. The response time of the mechanical shutter is on the order of several milliseconds, measured using an oscilloscope and a photodetector. The mechanical shutter with relay design is used in the repump laser optics. The speaker-based mechanical shutter has less uncontrolled bounce than the relay-based design.

3.3.1.3 Repump Laser

The repump laser, resonant with the $F = 1 \rightarrow F' = 2$ transition, is necessary for the MOT operation. It pumps the atoms in the $F = 1$ dark state back to the MOT cycling transition. The repump laser frequency is about 6.83 GHz higher than that of the MOT master laser.

The laser-locking method used for the repump laser is different from that used for

FIGURE 3.23: The mechanical shutter used for the pyramid MOT laser. It is mounted near the focus of a telescope system.

the MOT master laser. We directly modulate the repump laser current to produce the dispersive error signal that is used to lock the laser frequency. It is locked to the line corresponding to the $F = 1 \rightarrow F' = 1/2$ crossover transition (this line has the strongest signal), which is 78.5 MHz red of the repump $F = 1 \rightarrow F' = 2$ transition. To compensate for this frequency difference and to shutter the laser beam, we put the repump laser through an 80 MHz AOM (IntraAction ATM-801A2). The first-order beam from the AOM is split into two by a PBSC. The transmitted beam is combined with the pyramid-MOT slave-laser beam at another PBSC and then sent to the pyramid MOT. The reflected beam from the first PBSC is sent to the other input port of the six-beam MOT fiber splitter and distributed out the six output ports. Little power is needed in the repump laser beams ($\sim$ 0.18 mW in each of the six-beam MOT laser beams, $\sim$ 1.2 mW in the pyramid MOT laser beam), so no repump slave laser is necessary.

3.3.1.4 Barrier Laser

The barrier laser, locked to the ^{85}Rb $F = 3 \rightarrow F' = 3/4$ crossover transition, provides the barrier beam for our one-way optical barrier experiment. The barrier laser is the same as the repump laser except for the frequency. The saturated-absorption spectroscopy setup and laser-locking method are the same as those of the repump laser. The laser current is modulated to create the dispersive error signal. The output beam from the barrier laser is coupled into a polarization maintaining fiber and sent to the experiment. There is no AOM needed for frequency and intensity control. The barrier laser has a mechanical shutter (the same design as the one shown in Fig. 3.22, but with a plastic flag) installed in its optical path.

3.3.1.5 Electronics for the Diode Lasers

The precise operation of diode lasers requires a current-controller circuit and a temperature-controller circuit. The current-supply circuit is a modified version of a circuit designed by the group of Kirk Madison, which in turn was adapted from a circuit by Todd Meyrath [66]. It is based on a standard P-I-D (proportional, integral, and derivative) feedback loop and a buffered current output. The features of this current supply circuit include coarse and fine current adjustments, a current modulation input, and laser diode protection via a current limiter and an automatic shorting relay that shorts the contacts of the laser diode when the current is off. The central component of our temperature control circuit is the WTC3243 controller

from Wavelength Electronics, which is an analog P-I control loop hybrid circuit for use in stable temperature control applications. The temperature-control circuit has an analog temperature readout, provided by a temperature transducer (AD590 from Analog Devices). Since laser diodes are sensitive to electric shocks, we add protection circuitry on every laser. The basic idea is to use several forward- and reverse-biased diodes to prevent the voltage from swinging too high in either direction [66]. All of the diode-laser controllers are home-made.

We built diode-laser lock boxes to implement active laser frequency stabilization. Each lock box includes an integrated lock-in amplifier, a 200 kHz local oscillator, a ramp generator for piezo scanning, a slow P-I feedback with high current drive capability for the piezo stack, a fast P-I-D feedback for injection current modulation, and an adjustable-gain feed-forward to the injection current for mode-hop-free laser tuning.

3.3.2 Dipole Trap Laser

In order to perform the experiment with neutral atoms, it is necessary to trap them. The traps for neutral atoms can be realized in three different ways: radiation-pressure traps (like MOTs), magnetic traps, and optical dipole traps.

Optical dipole traps rely on the electric dipole interaction with inhomogeneous electric fields, normally from far-detuned light. Typical trap depths are in the range below one mK. Optical dipole traps do not require magnetic fields and are relatively easy to set up, thus making them ideal for creating a conservative and tightly confining

trapping potential. The optical excitation for a far-off-resonance dipole trap (FORT) can be extremely low, so the optical dipole traps will not disturb the atoms severely like MOTs do. The trapping is independent of the particular sub-level of electronic ground state for normal trap configuration which uses linearly polarized light. The internal ground-state dynamics can be exploited on a time scale of many seconds. For all the reasons presented here, we selected optical dipole trap for our experiment.

In our experiment, the atoms are put into a conservative optical dipole trap with negligible spontaneous emission (the maximum photon scattering rate is $R_{\text{scatter}} \simeq 2$ s^{-1}). A far-off-resonance laser is used to produce the optical dipole trap. The laser used in our experiment is a 1090 nm Ytterbium-doped fiber laser from SPI Lasers (Model SP-M-20-A-1090-N-20-DC). The fiber laser has a maximum power of 20 W and a $\sim$ 5 mm collimated output beam diameter. The CW output can be modulated at frequencies up to 50 kHz. This fiber laser has an emission linewidth FWHM of less than 2 nm and a random polarization (when we rotate the fiber laser head through 360° and pass the laser beam through a polarizer, the transmitted power varies by less than 20%). The output power variation over a 12 hour period is smaller than 2%.

The fiber laser is mounted on a 100 mm travel linear air bearing stage (Aerotech ABL 10100-LT) as shown in Fig. 3.24. In our experiment, we focus the collimated Gaussian beam from the fiber laser to a 31.0(5) μm waist ($1/e^2$ intensity radius) with a 2.8 mm Rayleigh length. The output power of the fiber laser is set to 10.0(5) W

(the power entering the Hellma cell is about 9.3 W). The fiber laser is an OEM laser. It only came with a laser head and the current supply. In order to operate the fiber laser conveniently, we built a fiber laser control box (Fig. 3.25).

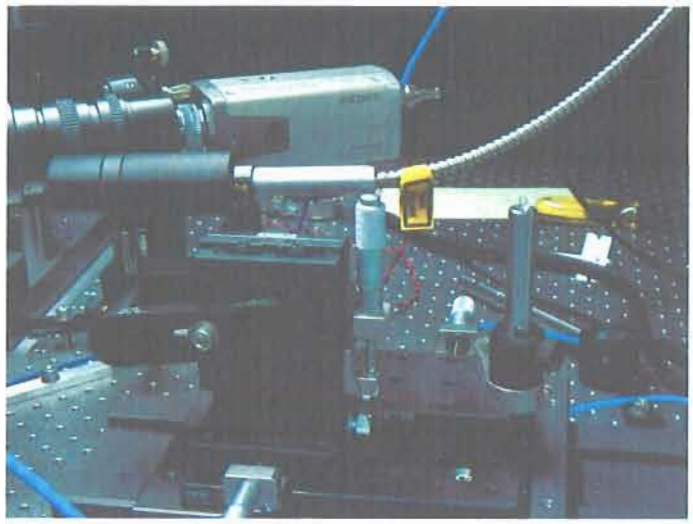

FIGURE 3.24: The fiber laser is mounted on a two-dimentional translation stage which sits on a 100 mm travel linear air bearing stage. A lens is attached to the fiber laser head via a lens tube to focus the fiber laser.

The maximum potential depth is $U_{\text{dipole}} \simeq k_{\text{B}} \cdot 1$ mK for ^{87}Rb atoms in either hyperfine ground level. The maximum photon scattering rate is $R_{\text{scatter}} \simeq 2\ \text{s}^{-1}$, which is so slow that the dipole potential is nearly conservative.

The optical dipole trap used in our experiment has the axial and radial harmonic frequencies of 25 Hz and 3.1 kHz, respectively. This dipole trap gives tight radial confinement, but weak confinement in the axial direction. We should note that the dipole trap is highly anharmonic at the edges. Due to the large difference in the axial

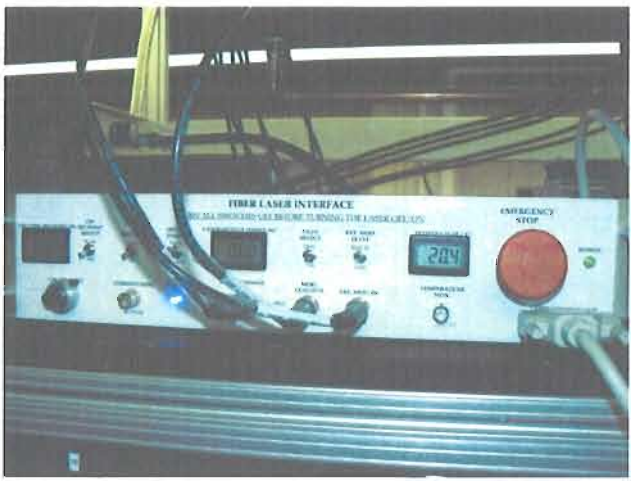

FIGURE 3.25: The fiber laser control box, which controls the fiber laser and acts as a modulation interface.

and radial oscillation frequencies, the atom motion can be regarded to be effectively one-dimensional along the dipole-laser beam axis.

3.4 Magneto-Optic Trap

There are three elements in a MOT: lasers, a vacuum chamber, and magnetic fields. In this section, we first describe the pyramid MOT, then we discuss the six-beam MOT. In both cases, we use anti-Helmholtz coils to create the magnetic quadrupole field and Helmholtz coils to compensate for external magnetic fields.

3.4.1 Pyramid MOT

Our pyramid MOT works as a source of pre-cooled atoms with which to supply the six-beam MOT in the science chamber. We chose a pyramid MOT because it is simple and reliable. The pyramid MOT configuration was originally demonstrated by

K. I. Lee *et al.* [52]. By adding a small hole at the vertex of the pyramid, the Foot group at Oxford made a continuous source of slow atoms with both Cs and Rb [67].

The pyramid in our setup consists of a set of four mirrors in the shape of an inverted pyramid (see Fig. 3.26). A hole at the vertex allows the cold atoms to travel to the second MOT. When the laser polarization is circular and is sent into the pyramid, the reflections from the mirrors of the pyramid produce three pairs of counterpropagating beams that have the same polarization configuration as that of a six-beam MOT. In the trapping region, the laser beams counterpropagating in each direction have opposite polarizations (σ^+ and σ^-). Fig. 3.26 shows the pyramid and the polarization configurations.

To create a magnetic field with a zero in the center and a linear gradient through the center region, two coils are arranged in the anti-Helmholtz configuration. The coils are wound with 23 AWG, heavy polyimide-ML insulated magnet wire from MWS around circular aluminum frames. After each layer of winding, a layer of 353ND high-temperature epoxy from Epoxy Technology is applied. The coils and epoxy can withstand temperatures up to 225°C. For a current of 1.3 A, the coils generate a gradient of about 11 G/cm, with a power dissipation of about 18 W. The coils get quite warm, but water-cooling is not necessary.

3.4.2 Six-beam MOT

The pyramid MOT works as a cold-atom source for the second MOT in a separate UHV chamber where the experiment is conducted. The second MOT follows the

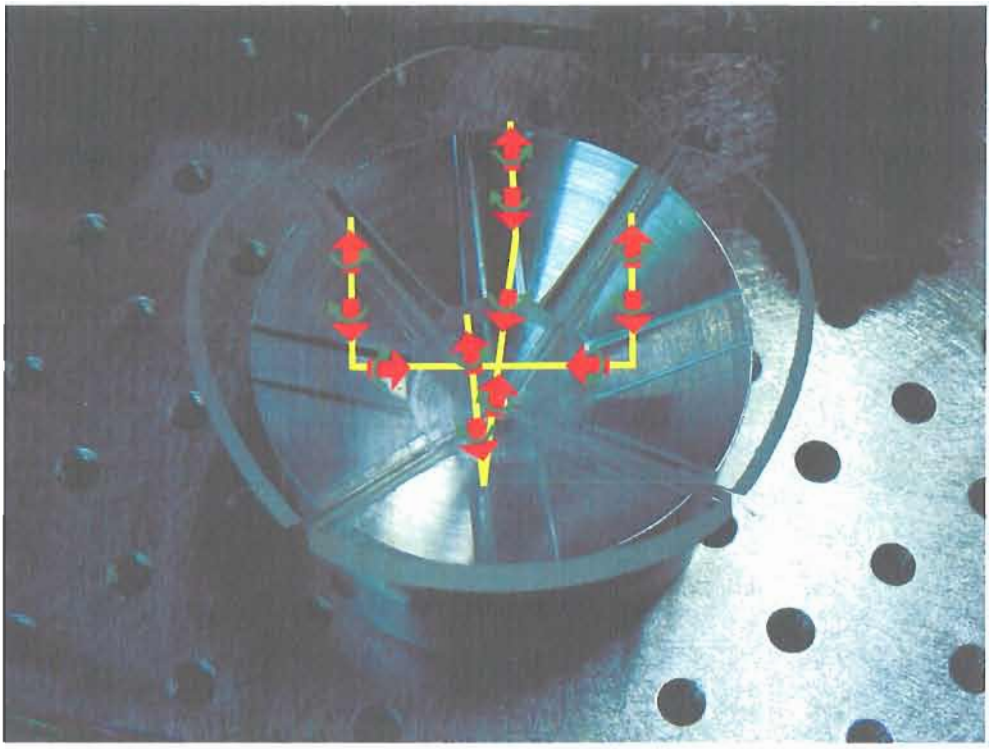

FIGURE 3.26: A model of the pyramid MOT optics. The image shows the pyramid and laser polarization configurations. Note that the laser configurations similar to those in standard six-beam MOT are automatically produced in this system.

ordinary six-beam MOT configuration: four laser beams (two pairs) are aligned in the horizontal plane, and two lasers (the third pair) are aligned in the vertical direction. For every pair of lasers, the polarization is set to σ^+/σ^-, and the two beams counterpropagate.

The magnetic-field coils to create the quadrupole magnetic field for the six-beam MOT are arranged in the anti-Helmholtz configuration and fit around the Hellma cell. The frame is made of Delrin, and are removed for a 200 °C bake-out.

To compensate for the external magnetic fields, two sets of three pairs of magnetic-field coils (each pair in the Helmholtz configuration) are placed around the pyramid MOT and the six-beam MOT. In our experiment, we also use Helmholtz coils to move the MOT to different initial positions inside the optical dipole trap.

3.5 Imaging System

In our experiment, a charge-coupled-device (CCD) camera is the main instrument for acquiring data. The atoms are imaged with a CCD camera, a MicroLine-ML402ME from Finger Lakes Instrumentation (Fig. 3.27). This camera can be externally triggered. It is equipped with a macro lens (Nikon Micro-Nikkor 55 mm, 1:3.5).

There are also two CCD cameras (Sony Exwave HAD video camera, Model No. SSL-M383) to monitor the atomic cloud in the first MOT and the second MOT

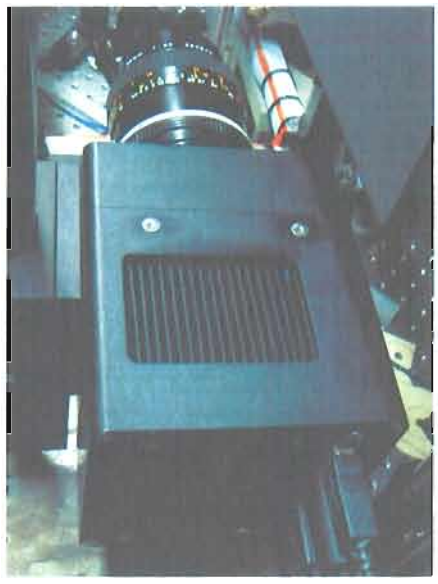

FIGURE 3.27: The MicroLine CCD camera equipped with a macro lens used to image atoms.

(Fig. 3.28). They are equipped with 6× zoom lens (Edmund Industrial Optics NT52-274). The images of the atomic cloud are displayed on LCD monitors.

Another camera used in our experiment is the Petcam (Panasonic BL-C1). After some modification, this network camera works as an inexpensive homemade beam profiler to measure the separation between two laser beams (Fig. 3.29). We removed the lens and glued a mount for ND (neutral density) filters to the front of the camera.

3.6 Control Electronics

Standard data acquisition and control systems are widely used in quantum-optics and cold-atom labs to automate the experiments. Many groups use National

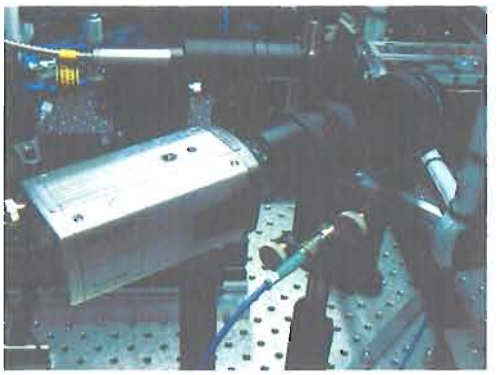

FIGURE 3.28: The CCD camera with zoom lens to monitor the atomic clouds.

FIGURE 3.29: The Petcam works as an inexpensive beam profiler.

Instruments hardware and LabView software for data acquisition and instrument control. The experiment control system used in our laboratory is named ZOINKS: "Zee Open Interface Networked Kontrol System." The ZOINKS project is a collaboration between our lab at the University of Oregon and the Madison Lab at the University of British Columbia. Some of the electronics are based on the designs by Todd Meyrath and Florian Schreck at the University of Texas at Austin. The ZOINKS equipment in our lab was designed, built and programmed by Peter Gaskell and Jeremy Thorn following the general framework by Daniel Steck.

The goal of ZOINKS is to develop an open-source set of hardware and software tools for controlling experiments in physics labs, especially in the area of quantum optics and cold-atom physics. The objective is to create a platform-independent lab control system. The components used for ZOINKS are relatively inexpensive, and the software development tools are open-source. ZOINKS does not rely on expensive proprietary products, such as the National Instruments hardware and software. ZOINKS not only saves a lot of money on product purchase and service fees, but also gives us much higher flexibility to design and troubleshoot our own lab control system.

The center piece of ZOINKS is an Ethernut board (Egnite GmbH Ethernut v. 2.1), which is an Ethernet-enabled embedded system that can be used to connect custom hardware directly to a network. Currently we are using Ethernut 2.1, which is

based on an ATmega128 microcontroller running at 14.7456 MHz, a 100 MBit SMSC Ethernet controller, and a 512 kB SRAM.

The hierarchy of components of ZOINKS has three levels: high-level devices, intermediate-level devices and low-level devices. Fig. 3.30 shows the structure of ZOINKS (figure from [68]).

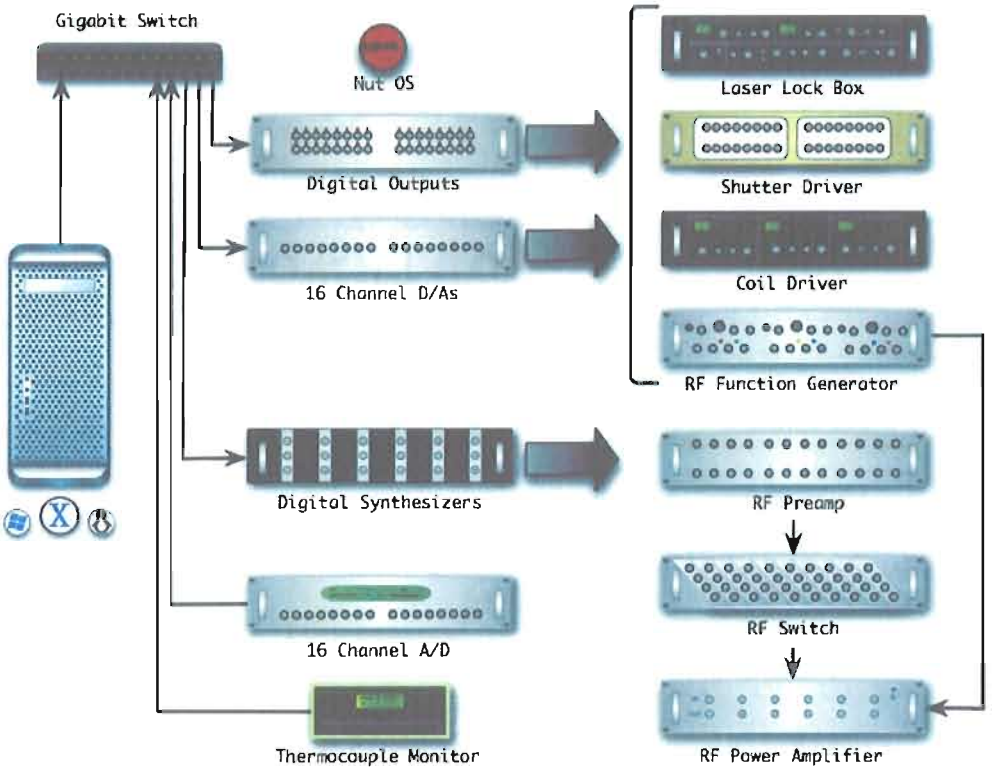

FIGURE 3.30: The structure of ZOINKS. The system includes a computer, Ethernut boards, UTBus-Ethernut interface boards, digital boxes, analog boxes, DDS, thermocouple monitors, and some other equipments that perform the experimental tasks, such as shutter driver, coil driver, RF function generator, etc. Adapted from [68].

High-level devices are programmed to execute certain sets of instructions.

Ethernut boards are the low-level devices. Intermediate-level devices are used to convert the instructions we write into the Ethernut board to the actual signals the instruments take. For example, the digital boxes and analog boxes are used to turn shutters or AOMs on or off following the instructions issued by the Ethernut board. Another example of an intermediate-level device is a Direct Digital Synthesizer (DDS), which is used to create an arbitrary sine wave for an AOM. Low-level devices are the instruments that perform the real tasks during the experiment, such as the mechanical shutters, AOMs, magnetic coils, or the CCD camera.

The general procedure of experimental run is as follows: First, the computer decides the timing of the experiment events; second, the computer sends commands to each high-level device, telling them when to perform various tasks; third, the high-level devices trigger intermediate-level devices to start the experiment (a Rb clock is used as an accurate timer); last, the intermediate-level devices run the low-level devices to perform the experiment.

CHAPTER IV

ONE-WAY BARRIER AND SINGLE-PHOTON COOLING

4.1 Introduction

In this chapter, we first discuss the limitations of present cooling schemes and the efforts exploring new cooling methods. Then we describe the model of a one-way barrier and show that it can increase the phase-space density of a sample and work as a general cooling method.

4.2 The Limitations of Standard Laser-Cooling Techniques

Laser cooling and trapping of neutral atoms has brought a revolution to the field of atom optics and is a common tool in the present research community. However, the standard laser-cooling techniques have serious limitations. Laser cooling of atoms depends on many photon scatterings. This requires a cycling transition, which limits the atoms to a small set of atoms in the periodic table. If there are no closed transitions, near-resonant radiation will optically pump the atoms into "dark" states well before they are cooled.

It is appealing to have a general method applicable to cooling most atoms, or even molecules. There are some elegant ideas that propose general cooling methods.

Two groups independently proposed a cooling mechanism called "cavity cooling," which relies on photon momentum transfer but does not require a cycling transition [69, 70]. Maunz *et al.* [71] demonstrated cavity cooling of single rubidium atoms stored in an intracavity dipole trap. The basic idea of cavity cooling is that the kinetic energy of the atoms or molecules is extracted from the coupled atom-cavity or molecule-cavity system via the cavity's photon loss channel. In Doppler cooling, the relevant energy detuning is between the incident laser beam and the atom. In cavity cooling, the relevant detuning is between the incident laser beam and the cavity resonance. If the incident laser is detuned slightly below the cavity resonance, the scattered light will be at the cavity resonance frequency in the preferred photon scattering events. The laser frequency and cavity resonance can be far off atomic or molecular resonance frequency, so this cooling scheme does not rely on the internal energy structures, thus permitting cooling of both atoms and molecules.

In the next sections of this chapter we will describe a one-way optical barrier, which in principle is a general laser-cooling method without requiring optical cavities.

4.3 One-Way Barrier

Recently Raizen and collaborators proposed a one-way barrier to implement a new laser cooling scheme [18]. The one-way barrier is an asymmetric optical potential barrier for atoms. Atoms see a different optical potential depending on which side of the barrier the atoms are located. By sweeping a one-way barrier across an

atomic trap, the phase-space density of the atomic sample can be compressed and the atomic sample can be cooled. Ruschaupt and Muga independently proposed a one-way barrier model (they call it an "atom diode") using stimulated Raman adiabatic passage [19]. The atom diode combines state-selective mirrors and pumping lasers to let the atoms pass in one direction but not in the opposite direction.

4.3.1 The Model of the One-Way Barrier

The one-way barrier model discussed here follows the idea of Raizen [18]. Alkali atoms are widely used in the area of cold atoms for the simplicity of their energy structure. For alkali atoms, the one-way barrier can be constructed as shown in Fig. 4.1. There are two ground states $|1\rangle$ and $|2\rangle$ and one excited state $|3\rangle$. The one-way barrier consists of two laser beams: beam RES is on resonance with the $|1\rangle \rightarrow |3\rangle$ transition, and beam M is set to the blue of the $|2\rangle \rightarrow |3\rangle$ transition and the red of the $|1\rangle \rightarrow |3\rangle$ transition. For atoms in state $|1\rangle$ the beam M is attractive, so the atoms will pass through beam M. The state of the atoms is changed to $|2\rangle$ by the optical pumping of beam RES. The state $|2\rangle$ is not influenced by beam RES (if it has any effect, it helps as a weak repulsive potential). Beam M acts as a repulsive potential for the atoms in state $|2\rangle$, thus blocking the transmission from right to the left. In our experiment, we tune the beam M between the $F = 1 \rightarrow F'$ and $F = 2 \rightarrow F'$ transitions of ^{87}Rb. Beam RES is set to the MOT repumping transition frequency.

The one-way barrier can be used to compress the phase-space density of an atomic gas. Consider a one-dimensional box with a spatially uniform distribution of atoms.

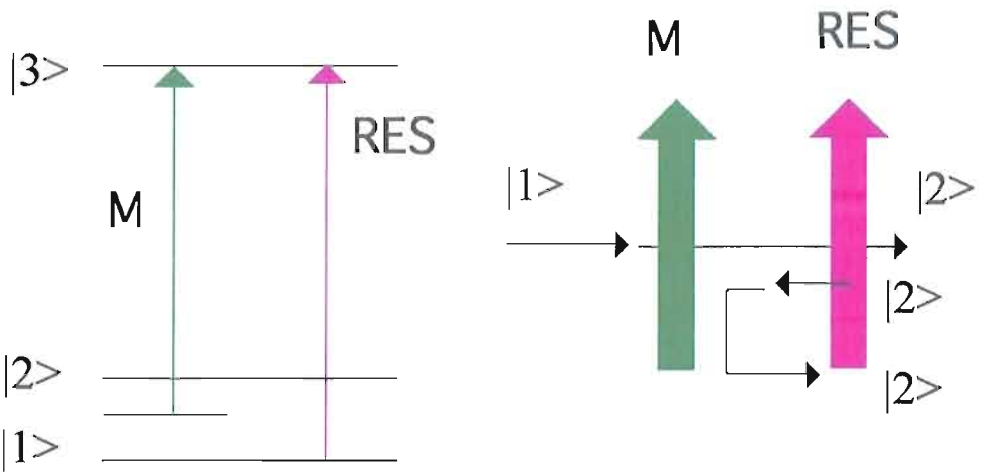

FIGURE 4.1: The simple model of one-way barrier for an alkali atom. Beam M is tuned to the blue of the atomic transition $|2\rangle \rightarrow |3\rangle$. It creates a repulsive barrier for atoms in ground state $|2\rangle$, but an attractive potential for atoms in ground state $|1\rangle$. Beam RES is tuned to the atomic resonance $|1\rangle \rightarrow |3\rangle$. It pumps the atoms from $|1\rangle$ to $|2\rangle$. Adapted from [18].

Suppose we put the one-way barrier somewhere in the box. After the one-way barrier is turned on, all the atoms will ideally accumulate on one side and the phase-space volume is compressed, assuming the momenta are not changed on average during the process.

4.3.2 Single-Photon Atomic Cooling

We discussed the limitations of traditional laser cooling and trapping methods, the efforts to develop new cooling techniques to produce cold atoms and molecules, and also the one-way barrier. Next we outline the general idea of single-photon atomic cooling based on the one-way barrier, as presented by Ruschhaupt *et al.* [72]. The term "single-photon atomic cooling" was coined by Raizen, and the experiment was demonstrated by his group [73].

Suppose the atoms are trapped in a harmonic trap as shown in Fig. 4.2. The one-way barrier intersects with the harmonic trap and sweeps slowly through the harmonic trap potential during the cooling process. After an atom passes through the one-way barrier, it scatters a photon. The photon scattering causes an irreversible change in the potential that traps the atom. If the one-way barrier sweeps slowly, it captures the atoms near their classical turning points, where they have very little kinetic energy. The slowly moving one-way barrier will adiabatically transport the atoms to the bottom of the potential without increasing their kinetic energy. A simple analogy for this situation is slowly moving a tennis racket downwards with a tennis

ball resting on it. The ball does not gain kinetic energy. By sweeping a one-way barrier through the trap, the atoms are cooled.

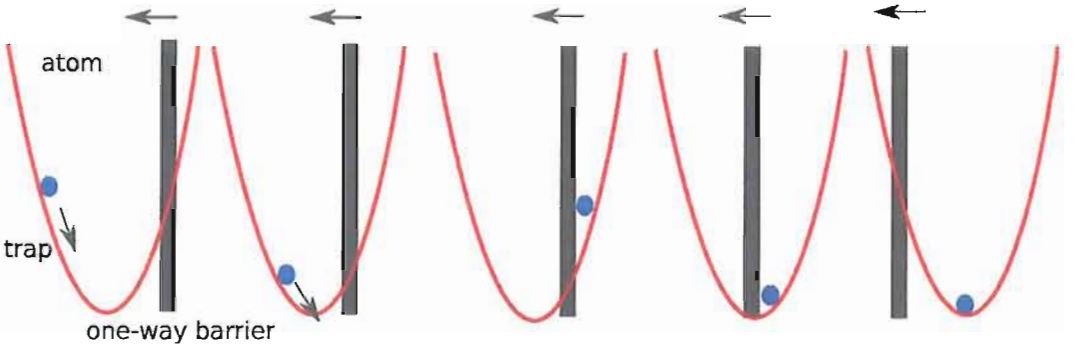

FIGURE 4.2: The schematic representation of the single-photon cooling method based on a one-way barrier. The atoms can pass the one-way barrier from left to right. The sequence of the 5 figures from left to right denotes the time evolution of the one-way barrier sweeping. Adapted from [72].

The important difference between the scheme here and the ordinary laser cooling is as follows: In ordinary laser cooling, the repeated scattering of photons is used to slow atoms, i.e. photon momentum transfer causes the cooling. In the cooling scheme described here, each atom in principle only scatters on average one photon. The entropy of the atoms is decreased and the atoms are cooled at the cost of the scattered photons. The scattering of a photon by each atom increases the entropy of the radiation field. In principle, all of the scattered photons can be detected. By taking into account the information gathered by photon detection, we can see the second law of thermodynamics will hold as expected. So the single-photon atomic cooling scheme is basically information cooling as proposed by Szilard [25].

After an atom passes through a one-way barrier, the one-way barrier will heat

the atom by a single photon recoil $(\hbar k)^2/2m$. This disturbance imposes one of the fundamental limitations to cooling via optical one-way barriers.

CHAPTER V

EXPERIMENTAL REALIZATION OF A ONE-WAY BARRIER

5.1 Introduction

In this chapter, we describe the one-way barrier [18, 19, 74, 75, 72, 76, 77, 78, 79, 80, 73] experiment, which demonstrates an asymmetric optical potential barrier for ultracold ^{87}Rb atoms [81].

The optical one-way barrier in our experiment consists of two focused laser beams. The first beam is tuned to have a red detuning from the $F = 1 \rightarrow F'$ hyperfine transitions, and a blue detuning from the $F = 2 \rightarrow F'$ hyperfine transitions. The second beam is locked to the ^{87}Rb repump transition $F = 1 \rightarrow F' = 2$. The optical dipole potential is proportional to $I(r)/\Delta$, where $I(r)$ is the local laser intensity, $\Delta = \omega_l - \omega_a$ is the laser frequency detuning, ω_l is the laser frequency, ω_a is the atomic resonance frequency. Since the laser frequency detunings with respect to the two ground level atomic resonances have opposite signs, the main barrier beam behaves as a potential well to atoms in the $F = 1$ ground state and as a potential barrier to the atoms in the $F = 2$ ground state. So the first beam (main barrier beam) will let the atoms in the $F = 1$ ground state transmit through it, but block the atoms in

the $F = 2$ ground state instead. The second beam (repumping barrier beam), which is aligned to the side of the main barrier beam and tuned to the repump transition, will pump the atoms from the $F = 1$ state to the $F = 2$ state, thus creating the asymmetry (see Fig. 5.1). If we start with all the atoms in the $F = 1$ ground state, they can pass through the main barrier beam. After the atoms pass through the main barrier beam, they are optically pumped into the $F = 2$ ground state by the repumping barrier beam. Now the main barrier beam presents a potential barrier to the atoms, and the atoms will be reflected from the barrier. The experiment clearly shows the transmission of atoms from one side to the other side and the reflection from that side.

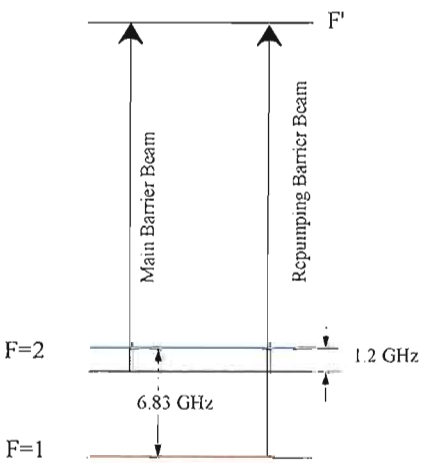

FIGURE 5.1: The energy level diagram for one-way barrier.

5.2 One-way Barrier Experimental Setup

The cold atoms in the optical one-way barrier experiment are collected using the setup described in Chapter III. Here we only describe the parts specifically for the optical one-way barrier experiment.

After we collect the cold atoms using a standard six-beam magneto-optic trap (MOT), we load the atoms into an optical dipole trap created by the fiber laser (described in Chapter III).

We use a small table to hold the one-way barrier optics, including two fiber couplers, a 50-50 beam splitter, an anamorphic prism pair, mirrors, and a lens. The optical layout on the small table is shown in Fig. 5.2. This table improves the stability of the one-way barrier optics and allows them to be moved elsewhere for calibration.

5.3 Dipole Trap Loading

The first step of our experiment is to load the cold atoms from the MOT into the dipole trap. Loading a FORT from a MOT is a dynamical process rich in interesting physics [82]. The experiment setup is shown schematically in Fig. 5.3. The starting point of the experiment is the six-beam MOT, described before in Chapter III. The ultra-high vacuum pressure inside the Hellma cell is $\lesssim 10^{-11}$ torr, which is critical for the experiment.

The sequence of loading the optical dipole trap from the MOT is as follows. First

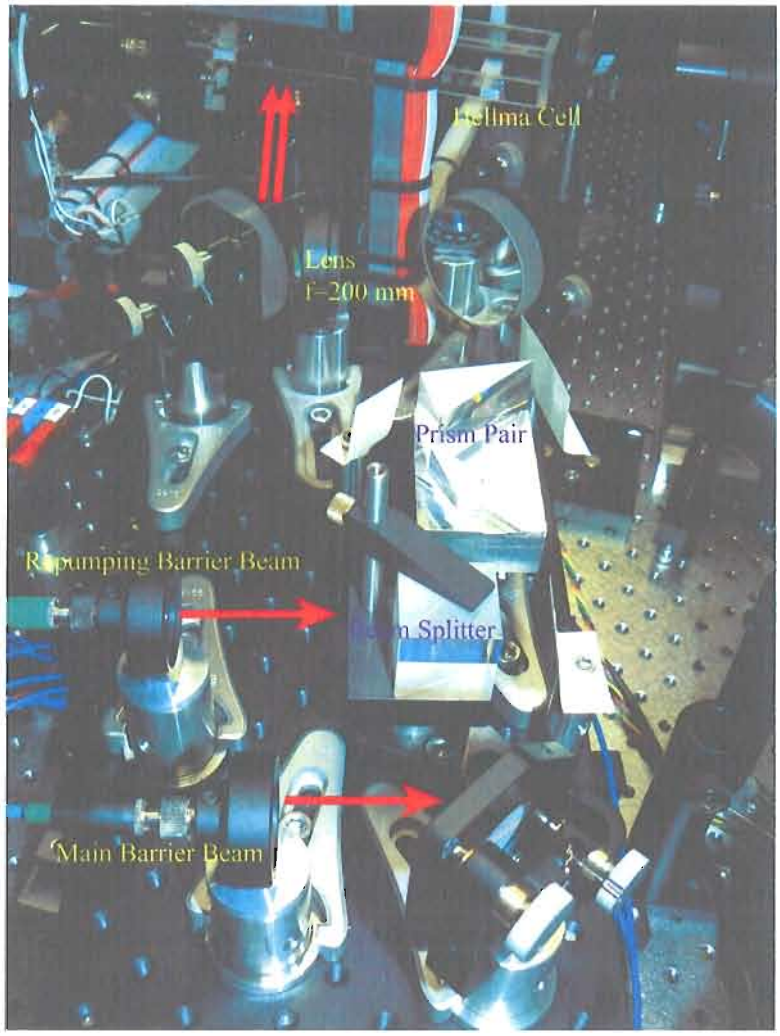

FIGURE 5.2: The optical layout of the one-way barrier beams on the small table. The main and repumping barrier beams are combined together using a 50-50 beam splitter. Then they pass through a prism pair to make the beam asymmetric. Finally the two beams go through a plano-convex lens ($f = 200$ mm) and overlap with the dipole trap beam. Their foci nearly coincide with the focus of the dipole trap beam. The separation between the two beams at the foci is adjusted to about 34 μm.

we load the MOT, then we increase the MOT laser detuning and reduce the light intensity to implement polarization-gradient cooling. After this secondary cooling stage, we have about 2×10^5 atoms at about 30 μK. Then we turn on the fiber laser and overlap it with the MOT. When we turn on the fiber laser, we simultaneously decrease the detuning of the MOT light, reduce the repump light intensity and recover the MOT light intensity to the original value. After a period of dipole loading time (normally 5 ms), we turn off the MOT light, repump light, and magnetic coils. In our experiment we load the dipole trap for 5 ms, and trap about 3×10^4 atoms at $\sim$ 100 μK. The longer loading time can trap more atoms, but at the same time the atoms will spread throughout the dipole trap. In order to resolve the atomic dynamics with localized initial conditions, we use a relatively short loading time. By shifting the MOT with a magnetic bias field created by the Helmholtz coils, we load the atoms 0.95 mm to either side of the dipole trap focus. To overlap the focus of the dipole trap with the MOT atoms, we observe the image taken by a CCD camera (Sony Exwave HAD video camera SSL-M383). When the overlap is optimized, the hole created by the dipole laser is centered on the image of the MOT atoms.

5.4 Experimental Demonstration of a One-way Barrier

The two one-way barrier beams are aligned parallel to each other and separated by 34(1) μm. Their foci nearly coincide with the dipole-trap focus. The two beams intersect the dipole-trap laser beam at about 12° from the perpendicular direction to

the dipole-trap beam axis. The optical setup is shown in Fig. 5.3. In order to make two optical sheets, we use an anamorphic prism pair to change the beam shape of the barrier beams. The resulting profiles of the two barrier beams are asymmetric Gaussian beams, with waists of 11.5(5) μm and 13(2) μm along the dipole-trap axis and 80(7) μm and 60(7) μm perpendicular to the dipole-trap axis for the main barrier beam and repumping barrier beam, respectively. The anamorphic prism pair expands the two beams horizontally. After focusing, the two beams are focused more in the horizontal direction than in the vertical direction. The alignment of the two barrier beams is critical to our experiment. Any small disturbance or bump of the small optical table, optics, or fiber coupler could change the alignment.

Originally we used the commonly used knife-edge method to measure the beam waists and the separation between the two barrier beams. When the intensity profile of the laser beam is Gaussian, the total intensity transmitted changes according to the error function as the knife-edge position varies. Determining the beam parameters requires a curve fit to the error function. We mounted a razor blade on the air bearing translation stage, with the laser beams propagating perpendicular to the moving direction of the translation stage. When the air bearing translation stage is moving, we record the integrated beam profiles by measuring the laser intensity on a detector as a function of the position of the translation stage. The beam waists and beam separation are calculated by fitting the data. We also use the Petcam to measure the separation between the barrier beams. We calibrated the Petcam by

comparing measurements with measurements from the air bearing translation stage.

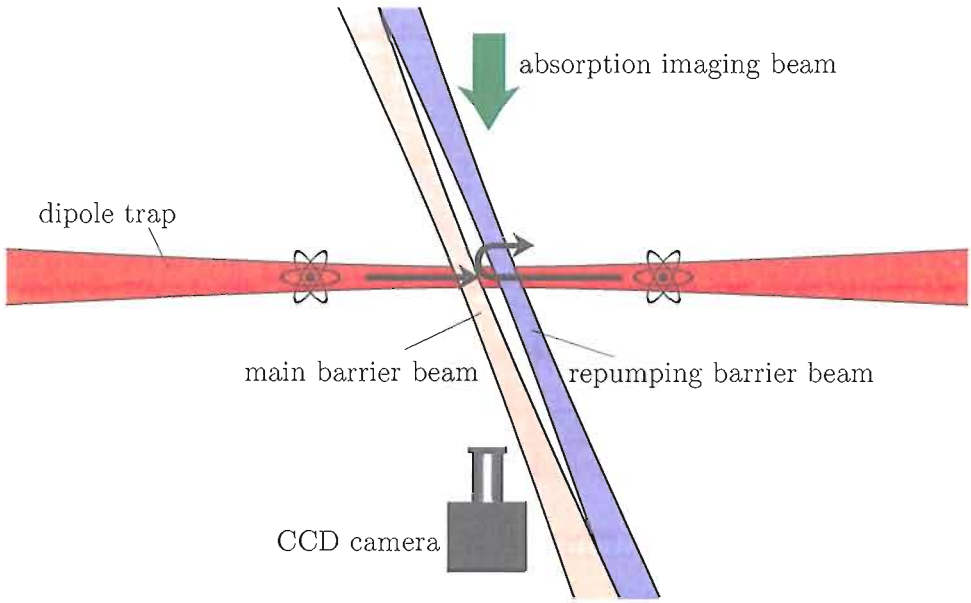

FIGURE 5.3: The two barrier beams, dipole trap beam, absorption imaging beam, and imaging system are shown in this schematic diagram of our optical setup. The two barrier beams are aligned parallel to each other and intersect the focus of the dipole trap beam at about 12°. The imaging beam is nearly perpendicular to the dipole-trap beam. The drawing was created by D. Steck.

To overlap the foci of the barrier beams with the MOT atoms (also the focus of the dipole trap), we move the small table back and forth, and use a mirror on the small table to steer the barrier beams after they are focused by the lens, then we use the atoms' image taken by the CCD camera to find the optimum position. The final step of alignment is done by dropping the atoms in the dipole trap and measuring the reflections from the main barrier beam. When the main barrier beam is locked to the repump line of ^{87}Rb and the alignment is good, good reflections are observed.

The repumping barrier beam is derived from the same laser source as the MOT repump laser, and has the same spectral properties. It is resonant with the MOT repump transition $F = 1 \rightarrow F' = 2$, and has a power of 0.36(4) μW as seen by the atoms. Note that the attenuation coefficients due to the cell are different for the two barrier beams. The polarization of the main barrier beam (repumping barrier beam) is vertical (horizontal), and we use a factor of 92% (94%) to take into account the attenuation. The main barrier beam is from a separate diode laser with its own saturated-absorption-spectroscopy-based frequency-stabilization setup. The frequency of the main barrier beam is stabilized to the ^{85}Rb $F = 3 \rightarrow F' = 3, 4$ crossover dip in the saturated absorption spectrum, which is 1.16(6) GHz blue of the ^{87}Rb MOT trapping transition ($F = 2 \rightarrow F' = 3$). The power of the main barrier beam is set to 40(4) μW as seen by the atoms. The two barrier beams are turned off during the dipole loading process.

The effect of the one-way barrier depends on the internal state in which the atoms are prepared. The main barrier beam works as a barrier for the atoms in the $F = 2$ state, but will permit the atoms in the $F = 1$ state to pass through it. In order to put the atoms into a particular state, we implement optical pumping. In our experiment, we turn off the MOT repump beam, which pumps the atoms to the $F = 2$ state, and leave the MOT trapping laser on for 7 ms, thus placing the atoms into the $F = 1$ ground state. Due to the optical transition selection rule, the decay $F' = 3 \rightarrow F = 1$ is forbidden. Thus, the frequency of the MOT trapping laser is detuned 70 MHz

to the red of the MOT trapping transition ($F = 2 \rightarrow F' = 3$) during the optical pumping process. This frequency detuning, which is combined with an AC Stark shift from the dipole trap (about 21 MHz), allows enough off-resonant coupling of the $F = 2 \rightarrow F' = 2$ transition to pump the atoms to the $F = 1$ ground state. By extinguishing the MOT trapping laser instead of MOT repump laser, the atoms can be pumped to the $F = 2$ ground state.

To detect the atom dynamics in the one-way barrier, a probe laser is used for absorption imaging. Absorption imaging is done by illuminating an atom cloud with a resonant laser beam that is absorbed by the atom cloud. The shadow cast by the atoms in the laser beam is imaged by the MicroLine CCD camera. The absorption image gives us the number and the position of atoms. The duration of the absorption imaging light (about 45 μs) is controlled by the pulse stabilization circuit and its frequency is resonant with the MOT trapping transition. We align the absorption imaging beam nearly perpendicular to the dipole trap beam, and use the MicroLine CCD camera to detect the absorption. The power fluctuations of the absorption imaging beam can result in poor subtraction of the background images. The background images are the bright dots and stripes resulting from the imaging beam flash. This problem is taken care of by the pulse stabilization circuit mentioned in Chapter III. Also we use an anamorphic prism pair to make the absorption imaging beam wider, thus allowing it to cover the full length of the dipole trap more uniformly.

The basic experimental procedure is as follows. We load the MOT and then

transfer the atoms from MOT into the dipole trap at certain positions by changing the magnetic bias field. After that, we turn off the MOT (anti-Helmholtz MOT coils and the MOT lasers), releasing the atoms into the dipole trap. The atoms prepared in the $F = 1$ or $F = 2$ ground states are released from the left or right of the center of the dipole trap, with or without the one-way barrier beams. We wait for half a oscillation period before turning on the barrier beams to allow background atoms to fall away. The atoms are recorded using the absorption imaging beam at different times after the drop. During the imaging process, the dipole trap is turned off. The 45 μs short absorption imaging pulse illuminates the atoms while they are effectively frozen in place (the oscillation period of atoms in the dipole trap is about 48 ms). The imaging procedure is destructive, so we need to repeat the cycle of loading, dropping, and imaging. By imaging the atoms at different times, we study the time evolution and dynamics of the atoms.

The main results of the one-way barrier are shown in Fig. 5.4. The four columns labeled from (a) to (d) shows the spatial distributions of atoms inside the dipole trap in response to the one-way barrier. The dipole-trap focus, which is nearly overlapped with the barrier beams, is located at the plot centers. Each curve is an average of 78 experiment repetitions.

Fig. 5.4(a) shows the evolution of atoms prepared in the $F = 1$ state and dropped from the left of the dipole trap with no barrier present. The atoms oscillate back

and forth inside the dipole trap. Some diffusion of the atomic cloud is due to the anharmonicity of the dipole trap.

The effect of the one-way barrier is demonstrated in Fig. 5.4(b). The atoms are prepared in the $F = 1$ state and loaded to the left of the dipole-trap center. (In the experiment, we load the atoms on the right side of the dipole trap, then let the atoms travel to the left, and then turn on the barrier. This approach eliminates artifacts due to any remaining background atoms by giving time for them to fall away under gravity.) The main barrier beam is to the left in the figure and the repumping barrier beam is to the right in the figure. Correspondingly, the transmitting side of the barrier is to the left, and the reflecting side is to the right. After the atoms are dropped, they transmit through the barrier on the way to the right-hand side. When they return from the right, the atoms are blocked by the one-way barrier and reflect off of it. Gradually the atoms settle to a steady state to the right-hand side of the one-way barrier. After 100 ms, there are about 80% of the initially trapped atoms remaining in the dipole trap. The lifetime of the atoms on the right-hand side typically ranges from 300 to 500 ms, depending on the temperatures of the atoms.

Fig. 5.4(c) shows the evolution of atoms initially prepared in the $F = 2$ state and loaded to the left of the dipole trap center. We expect the atoms will reflect off from the barrier, since they are prepared in the "wrong" state $F = 2$. It turns out that is not the whole story. From Fig. 5.4(c), we can see that the atoms initially reflect off the barrier. But later on, the atoms gradually manage to go through the

barrier. Compared to the atoms in the $F = 1$ state, the atoms in the $F = 2$ state transmit through the barrier without much extra loss. The transmitting of atoms in the "wrong" state results from the optical pumping due to the main barrier beam. The main barrier beam is closer to the $F = 2 \rightarrow F'$ transition than to the $F = 1 \rightarrow F'$ transition, thus preferentially optically pumping the atoms into the transmitting state $F = 1$.

Fig. 5.4(d) shows what happens when we drop the atoms from the right-hand side of the barrier. The plots clearly shows the atoms bouncing off the barrier. The reflection is good for atoms in both the $F = 2$ and $F = 1$ states. It is easy to understand that the atoms in the $F = 2$ state will reflect from the barrier very nicely, since they are in the "reflecting" state. The clean reflection of atoms in "wrong" state $F = 1$ is again due to the optical pumping effect. The repumping barrier beam optically pumps the atoms into the $F = 2$ state before they encounter the main barrier beam, which will then block the transmission of atoms.

The loss of atoms are mainly due to the scattering from the barrier beams, both during the passing the main barrier beam and reflecting from it. The loss due to the main barrier beam is a limitation imposed by the use of ^{87}Rb: the 6.8 GHz ground-state hyperfine splitting limits the detunings of the main barrier beam to relatively small values. In principle, an atom crossing the one-way barrier needs to scatter only one photon in order to get through the barrier [18, 79, 73]. In our experiment, the

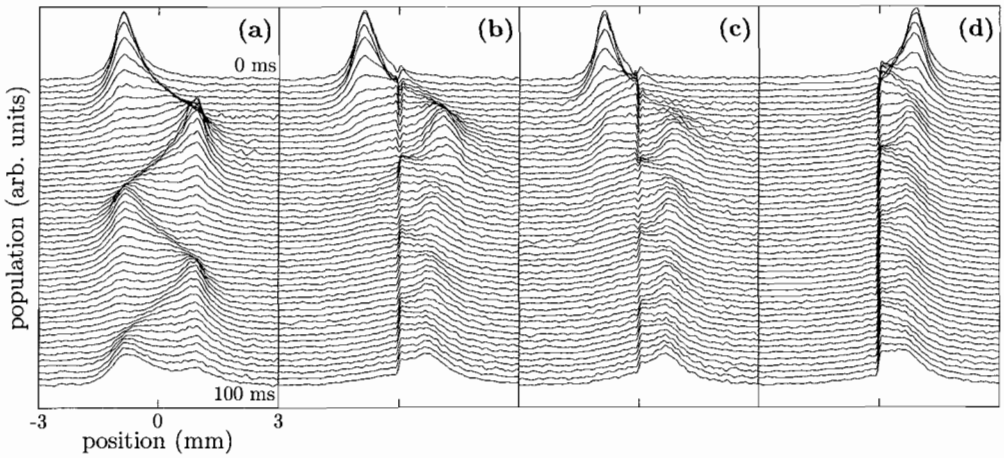

FIGURE 5.4: The spatial distributions of atoms in the dipole trap responding to the one-way barrier. Column (a): atoms initially prepared in the $F = 1$ state are dropped from the left without barrier present. Column (b): atoms initially in the $F = 1$ state are dropped from the left onto the barrier. Column (c): atoms initially in the $F = 2$ state are dropped from the left onto the barrier. Column (d): atoms initially in the $F = 1$ state are dropped from the right onto the barrier.

relatively small frequency detuning of the main barrier beam causes more scattered photons than necessary.

To estimate the number of photon scattering events, we assume the barrier has a peak potential U_0 and full width at half maximum w. The peak photon scattering rate is given by $R_{\text{scatt}} = |\Gamma U_0/\hbar\Delta|$, where Γ is the excited-state decay rate. The atoms hit the barrier with an initial kinetic energy, which is determined by the initial atomic displacement. We write the kinetic energy as $\eta|U_0|$, where η is the ratio of kinetic energy to the peak potential energy. The total number of scattering events is the photon scattering rate times the time the atoms take to pass the potential. It is on the order of $N_{\text{scatt}} \sim R_{\text{scatt}} w/v = w\Gamma\sqrt{m|U_0|}/\hbar|\Delta|\sqrt{2\eta}$, where $v = \sqrt{2\eta|U_0|/m}$ is the

speed of the atoms. We assume the speed to be constant here. Putting experimental parameters into this expression, using $w = 16$ μm for main barrier beam, $\eta = 2.2$, and $U_0 = -h \cdot 0.96(10)$ MHz, we find $\sim$0.7 scattering events for each transmission due to the main barrier beam. Due to the uneven detunings, $\eta < 1$ for the reflecting state, so atoms can be reflected. Taking into account the changes of atomic speed and atomic state change, we estimate $N_{\mathrm{sc}} \sim 1$ for transmission. When the repumping barrier beam is also included in the simulation, we find N_{sc} increases to about 3 during transmission and about 10 for a single reflection.

In order to reduce the photon scattering events, we could try to detune the barrier between the two transitions and keep the overlap between the two barrier beams minimal. This approach does not work, because there is no barrier height for which scattering during both transmission and reflection have sufficiently low scattering rates that the atomic states could be expected to not change. Atomic state changes are disastrous to the operation of the one-way barrier. We chose to tolerate some heating from the photon scattering in order to minimize the atomic state changes. This led to the current setup, where the barrier detuning pumps atoms into the transmitting state, and there is some overlap between beams to keep the atoms on the reflecting side in the reflecting state.

The evolution of atoms in Fig. 5.4(c) can be explained by the scattering from the main barrier beam. The main barrier beam preferentially pumps the atoms that should reflect off the transmitting side to the transmitting state $F = 1$. Atoms are

likely pumped to the $F = 1$ state while turning around, and thus moving slowly, leading to increased scattering and loss. (In experiment, we did not see much loss.)

5.5 Maxwell's Demon and Phase-Space Compression

Our experiment is a literal realization of Maxwell's demon. Fig. 5.5 shows the atom number on each side of the barrier as a function of time when we load the dipole trap symmetrically about the barrier location. We loaded the atoms away from the dipole trap center for 110 ms. The atoms (about 9×10^4) then uniformly and symmetrically filled the dipole trap. After letting the atoms equilibrate in the dipole trap for 200 ms, we turn on the barrier with a lower power of 18(2) μW. The barrier acts like the trapdoor operated by Maxwell's demon. It "opens" to let the atoms travel from left to right, but "closes" to prevent the atoms from traveling from right to left. The atoms gradually accumulate on the right-hand side (reflecting side) of the barrier. The result of atom evolution is atoms moves from the left side to the right side, so the physical space in which atoms reside is compressed. The spatial compression is countered by the heating due to the spontaneous photon scattering in the presence of the barrier. The phase-space density is observed to increase by about 7%. The phase-space density is defined as the number of trapped atoms per unit length (one-dimensional dipole trap in our experiment) per unit momentum. We think we can achieve better phase-space compression, but our experimental setup currently optimizes the barrier asymmetry instead of phase-space compression.

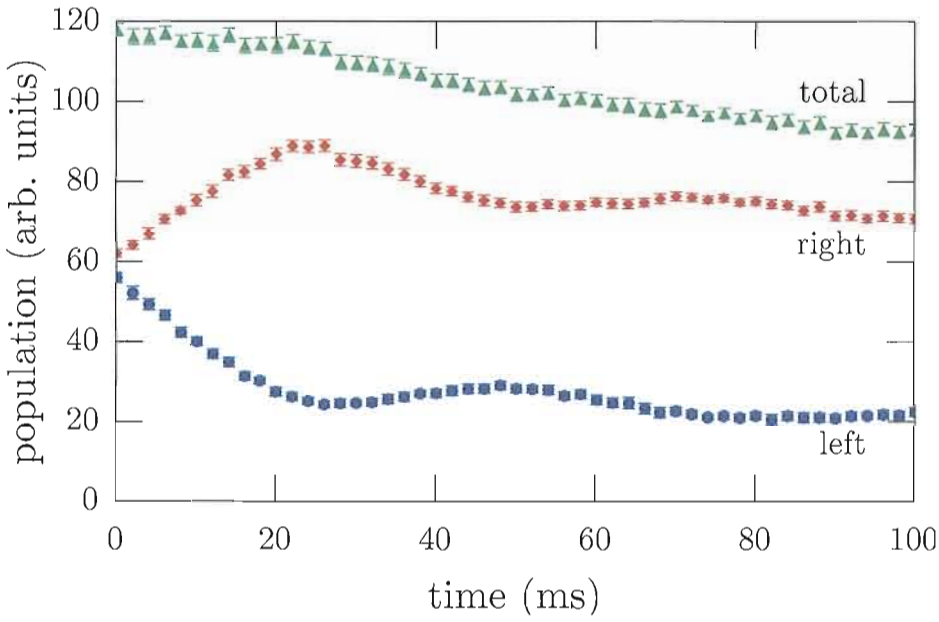

FIGURE 5.5: Atom populations on the left-hand side and right-hand side of the barrier and the total atom populations. The atoms are loaded throughout the dipole trap. The error bars indicate statistical error from averages over 38 repetitions at each time.

Our experiment does not violate the second law of thermodynamics. In order to let the atoms pass through the one-way barrier only in one direction, the demon must perform measurements to obtain the information of the internal states of the atoms. Due to the accumulated information, the entropy of the demon's memory increases, which balances the entropy decrease of the atoms. In a cyclic process, the demon must reset or "erase" its memory. The erasure requires work, in accordance with the second law of thermodynamics. In our experiment, the erasure occurs via the spontaneous scattering of a photon, which carries away the required entropy to reconcile our experiment with the second law.

CHAPTER VI

CONCLUSION

In this thesis, the design, construction and operation of an apparatus for atom-optics experiments has been described. This apparatus is versatile enough to accommodate many future projects.

An experimental demonstration of an optical one-way barrier has been reported in the second part of this thesis. This one-way barrier permits the atoms incident on one side transmitting through it, and prevents the atoms from going back. Such a "atom diode" device can be used as a tool for guiding and sorting atoms, which may find applications in "atom on a chip" technologies such as miniature atomic clocks. The one-way barrier is a also literal realization of Maxwell's demon. We achieved phase-space compression using the one-way barrier, which may have important implications for cooling atoms and molecules that can not be cooled by standard laser-cooling techniques.

BIBLIOGRAPHY

[1] S. Chu, "Nobel Lecture: The manipulation of neutral particles," Rev. Mod. Phys. **70**, 685 (1998).

[2] C. N. Cohen-Tannoudji, "Nobel Lecture: Manipulating atoms with photons," Rev. Mod. Phys. **70**, 707 (1998).

[3] W. D. Phillips, "Nobel Lecture: Laser cooling and trapping of neutral atoms," Rev. Mod. Phys. **70**, 721 (1998).

[4] C. S. Adams, M. Sigel, and J. Mlynek, "Atom optics," Phys. Rep. **240**, 143 (1994).

[5] P. Meystre, *Atom optics* (Springer Verlag, 2001).

[6] M. Takamoto, F.-L. Hong, R. Higashi, and H. Katori, "An optical lattice clock," Nature **435**, 321 (2005).

[7] C. Monroe, "Quantum information processing with atoms and photons," Nature **416**, 238 (2002).

[8] M. H. Anderson, J. R. Ensher, M. R. Matthews, C. E. Wieman, and E. A. Cornell, "Observation of Bose-Einstein condensation in a dilute atomic vapor," Science **269**, 198 (1995).

[9] K. B. Davis, M. O. Mewes, M. R. Andrews, N. J. van Druten, D. S. Durfee, D. M. Kurn, and W. Ketterle, "Bose-Einstein Condensation in a Gas of Sodium Atoms," Phys. Rev. Lett. **75**, 3969 (1995).

[10] C. C. Bradley, C. A. Sackett, J. J. Tollett, and R. G. Hulet, "Evidence of Bose-Einstein Condensation in an Atomic Gas with Attractive Interactions," Phys. Rev. Lett. **75**, 1687 (1995).

[11] B. DeMarco and D. S. Jin, "Onset of Fermi degeneracy in a trapped atomic gas," Science **285**, 1703 (1999).

[12] S. Chu, "Cold atoms and quantum control," Nature **416**, 206 (2002).

[13] I. I. Rabi, J. R. Zacharias, S. Millman, and P. Kusch, "A New Method of Measuring Nuclear Magnetic Moment," Phys. Rev. **53**, 318 (1938).

[14] N. Ramsey, "A New Molecular Beam Resonance Method," Phys. Rev. **76**, 996 (1949).

[15] K. Jacobs and D. Steck, "A Straightforward Introduction to Continuous Quantum Measurement," Contemporary Physics **47**, 279 (2007).

[16] D. A. Steck, K. Jacobs, H. Mabuchi, T. Bhattacharya, and S. Habib, "Quantum Feedback Control of Atomic Motion in an Optical Cavity," Phys. Rev. Lett. **92**, 223 004 (2004).

[17] D. A. Steck, K. Jacobs, H. Mabuchi, S. Habib, and T. Bhattacharya, "Feedback cooling of atomic motion in cavity QED," Phys. Rev. A **74**, 012 322 (2006).

[18] M. G. Raizen, A. M. Dudarev, Q. Niu, and N. J. Fisch, "Compression of atomic phase space using an asymmetric one-way barrier," Phys. Rev. Lett. **94**, 053 003 (2005).

[19] A. Ruschhaupt and J. G. Muga, "Atom diode: A laser device for a unidirectional transmission of ground-state atoms," Phys. Rev. A **70**, 061 604 (2004).

[20] B. T. Seaman, M. Kramer, D. Z. Anderson, and M. J. Holland, "Atomtronics: Ultracold-atom analogs of electronic devices," Phys. Rev. A **75**, 023 615 (2007).

[21] R. A. Pepino, J. Cooper, D. Z. Anderson, and M. J. Holland, "Atomtronic circuits of diodes and transistors," arXiv:0705.3268 (2007).

[22] J. Strnad, "The second law of thermodynamics in a historical setting," Phys. Educ. **19**, 94 (1984).

[23] R. P. Feynman, R. B. Leighton, and M. Sands, *The Feynman Lectures on Physics Vol. 1* (Addison-Wesley Publishing Company, 1964).

[24] J. C. Maxwell, *Theory of Heat* (Longmans, Green, and Co., 1871).

[25] L. Szilard, "On the decrease of entropy in a thermodynamics system by the intervention of intelligent beings," Z. Phys. **53**, 840 (1929).

[26] R. Landauer, "Dissipation and heat generation in the computing process," IBM J. Res. & Dev. **5**, 183 (1961).

[27] C. H. Bennett, "Demons, engines and the second law," Scientific American **257**, 108 (1987).

[28] H. J. Metcalf and P. van der Straten, *Laser Cooling and Trapping* (Springer, 1999).

[29] C. S. Adams and E. Riis, "Laser cooling and trapping of neutral atoms," Prog. Quant. Electron. **21**, 1 (1997).

[30] H. J. Metcalf and P. van der Straten, "Laser cooling and trapping of atoms," J. Opt. Soc. Am. B **20**, 887 (2003).

[31] J. Eschner, G. Morigi, F. Schmidt-Kaler, and R. Blatt, "Laser cooling of trapped ions," J. Opt. Soc. Am. B **20**, 1003 (2003).

[32] S. Chu, L. Hollberg, J. E. Bjorkholm, A. Cable, and A. Ashkin, "Three-dimensional viscous confinement and cooling of atoms by resonance radiation pressure," Phys. Rev. Lett. **55**, 48 (1985).

[33] J. Prodan, A. Migdall, W. D. Phillips, I. So, H. Metcalf, and J. Dalibard, "Stopping Atoms with Laser Light," Phys. Rev. Lett. **54**, 992 (1985).

[34] W. Ketterle, "Nobel lecture: When atoms behave as waves: Bose-Einstein condensation and the atom laser," Rev. Mod. Phys. **74**, 1131 (2002).

[35] E. A. Cornell and C. E. Wieman, "Nobel Lecture: Bose-Einstein condensation in a dilute gas, the first 70 years and some recent experiments," Rev. Mod. Phys. **74**, 875 (2002).

[36] R. Grimm, M. Weidemuller, and Y. B. Ovchinnikov, "Optical dipole traps for neutral atoms," Adv. At. Mol. Opt. Phys. **42**, 95 (2000).

[37] V. S. Letokhov, "Doppler line narrowing in a standing light wave," JETP Lett. **7**, 272 (1968).

[38] A. Ashkin, "Acceleration and trapping of particles by radiation pressure," Phys. Rev. Lett. **24**, 156 (1970).

[39] S. Chu, J. E. Bjorkholm, A. Ashkin, and A. Cable, "Experimental obaservation of optically trapped atoms," Phys. Rev. Lett. **57**, 314 (1986).

[40] T. Hänsch and A. Schawlow, "Cooling of gases by laser radiation," Opt. Commun. **13**, 68 (1975).

[41] D. Wineland and H. Dehmelt, "Proposed 1014 $\delta\nu < \nu$ laser fluorescence spectroscopy on Tl+ mono-ion oscillator III (side band cooling)," Bull. Am. Phys. Soc. **20**, 637 (1975).

[42] E. L. Raab, M. Prentiss, A. Cable, S. Chu, and D. E. Pritchard, "Trapping of Neutral Sodium Atoms with Radiation Pressure," Phys. Rev. Lett. **59**, 2631 (1987).

[43] C. Monroe, W. Swann, H. Robinson, and C. Wieman, "Very cold trapped atoms in a vapor cell," Phys. Rev. Lett. **65**, 1571 (1990).

[44] D. Haubrich, H. Schadwinkel, F. Strauch, B. Ueberholz, R. Wynands, and D. Meschede, "Observation of individual neutral atoms in magnetic and magneto-optical traps," Europhys. Lett. **34**, 663 (1996).

[45] D. W. Sesko, T. G. Walker, and C. E. Wieman, "Behavior of neutral atoms in a spontaneous force trap," J. Opt. Soc. Am. B **8**, 946 (1991).

[46] P. D. Lett, R. N. Watts, C. I. Westbrook, W. D. Phillips, P. L. Gould, and H. J. Metcalf, "Observation of Atoms Laser Cooled below the Doppler Limit," Phys. Rev. Lett. **61**, 169 (1988).

[47] J. Dalibard and C. Cohen-Tannoudji, "Dressed-atom approach to atomic motion in laser light: the dipole force revisited," J. Opt. Soc. Am. B **2**, 1707 (1985).

[48] J. Dalibard and C. Cohen-Tannoudji, "Laser cooling below the Doppler limit by polarization gradients: simple theoretical models," J. Opt. Soc. Am. B **6**, 2023 (1989).

[49] C. Cohen-Tannoudji and W. D. Phillips, "New mechanisms for laser cooling," Physics Today **43**, 33 (1990).

[50] W. D. Phillips and H. Metcalf, "Laser deceleration of an atomic beam," Phys. Rev. Lett. **48**, 596 (1982).

[51] C. J. Myatt, N. R. Newbury, R. W. Ghrist, S. Loutzenhiser, and C. E. Wieman, "Multiply loaded magneto-optical trap," Opt. Lett. **21**, 290 (1996).

[52] K. I. Lee, J. A. Kim, H. R. Noh, and W. Jhe, "Single-beam atom trap in a pyramidal and conical hollow mirror," Opt. Lett. **21**, 1177 (1996).

[53] K. M. Birnbaum and T. Q. O. Group, "Ultra-High Vacuum Chambers," (2005). `http://www.its.caltech.edu/~qoptics/Vacuum/UHV_chambers.pdf`.

[54] J. L. Hanssen, "Controlling Atomic Motion: From Single Particle Classical Mechanics to Many Body Quantum Dynamics," Ph.D. thesis, The University of Texas at Austin (2004).

[55] J. M. Lafferty, ed., *Foundations of vacuum sience and technology* (John Wiley, 1998), Ch. 2, p. 81.

[56] S. G. Cox, P. F. Griffin, C. S. Adams, D. DeMille, and E. Riis, "Reusable ultrahigh vacuum viewport bakeable to 240 °C," Rev. Sci. Instrum. **74**, 3185 (2003).

[57] C. E. Wieman and L. Hollberg, "Using diode lasers for atomic physics," Rev. Sci. Instrum. **62**, 1 (1991).

[58] K. B. MacAdam, A. Steinbach, and C. Wieman, "A narrow-band tunable diode laser system with grating feedback, and a saturated absorption spectrometer for Cs and Rb," Am. J. Phys. **60**, 1098 (1992).

[59] B. G. Klappauf, "Experimental Studes of Quantum Chaos with Trapped Cesium," Ph.D. thesis, The University of Texas at Austin (1998).

[60] D. A. Steck, "Quantum Chaos, Transport, and Decoherence in Atom Optics," Ph.D. thesis, The University of Texas at Austin (2001).

[61] W. H. Oskay, "Atom Optics Experiments in Quantum Chaos," Ph.D. thesis, The University of Texas at Austin (2001).

[62] C. Ye, *Tunable External Cavity Diode Lasers* (World Scientific, 2004).

[63] A. E. Siegman, *Lasers* (University Science Books, 1986).

[64] K. Singer, S. Jochim, M. Mudrich, A. Mosk, and M. Weidemüller, "Low-cost mechanical shutter for light beams," Rev. Sci. Instrum. **73**, 4402 (2002).

[65] T. P. Meyrath, "Inexpensive mechanical shutter and driver for optics experiments," (2003). `http://george.ph.utexas.edu/~meyrath/informal/shutter.pdf`.

[66] T. P. Meyrath, "An analog current controller design for laser diodes," (2003). `http://george.ph.utexas.edu/~meyrath/informal/laser%20diode.pdf`.

[67] J. Arlt, O. Marago, S. Webster, S. Hopkins, and C. Foot, "A pyramidal magneto-optical trap as a source of slow atoms," Opt. Commun. **157**, 303 (1998).

[68] P. Gaskell, "Zoinks open interface network kontrol system," `http://atomoptics.uoregon.edu/~zoinks/`.

[69] P. Horak, G. Hechenblaikner, K. M. Gheri, H. Stecher, and H. Ritsch, "Cavity-Induced Atom Cooling in the Strong Coupling Regime," Phys. Rev. Lett. **79**, 4974 (1997).

[70] V. Vuletić and S. Chu, "Laser Cooling of Atoms, Ions, or Molecules by Coherent Scattering," Phys. Rev. Lett. **84**, 3787 (2000).

[71] P. Maunz, T. Puppe, I. Schuster, N. Syassen, P. W. H. Pinkse, and G. Rempe, "Cavity cooling of a single atom," Nature **428**, 50 (2004).

[72] A. Ruschhaupt, J. G. Muga, and M. G. Raizen, "One-photon atomic cooling with an optical Maxwell demon valve," J. Phys. B: At. Mol. Opt. Phys. **39**, 3833 (2006).

[73] G. N. Price, S. T. Bannerman, K. Viering, E. Narevicius, and M. G. Raizen, "Single-photon atomic cooling," Phys. Rev. Lett. **100**, 093 004 (2008).

[74] A. M. Dudarev, M. Marder, Q. Niu, N. J. Fisch, and M. G. Raizen, "Statistical mechanics of an optical phase space compressor," Europhys. Lett. **70**, 761 (2005).

[75] S. W. Kim and M.-S. Choi, "Decoherence-driven quantum transport," Phys. Rev. Lett. **95**, 226 802 (2005).

[76] A. Ruschhaupt and J. G. Muga, "Adiabatic interpretation of a two-level atom diode, a laser device for unidirectional transmission of ground-state atoms," Phys. Rev. A **73**, 013 608 (2006).

[77] A. Ruschhaupt, J. G. Muga, and M. G. Raizen, "Improvement by laser quenching of an 'atom diode': a one-way barrier for ultra-cold atoms," J. Phys. B: At. Mol. Opt. Phys. **39**, L133 (2006).

[78] A. Ruschhaupt and J. G. Muga, "Three-dimensional effects in atom diodes: Atom-optical devices for one-way motion," Phys. Rev. A **76**, 013 619 (2007).

[79] G. N. Price, S. T. Bannerman, E. Narevicius, and M. G. Raizen, "Single-photon atomic cooling," Laser Phys. **17**, 965 (2007).

[80] A. Ruschhaupt and J. G. Muga, "Atom cooling with an atom-optical diode on a ring," arXiv:0801.2448v1 (2008).

[81] J. J. Thorn, E. A. Schoene, T. Li, and D. A. Steck, "Experimental realization of an optical one-way barrier for neutral atoms," Phys. Rev. Lett. **100**, 240 407 (2008).

[82] K. L. Corwin, "A Circularly-Polarized Optical Dipole Trap and Other Development in Laser Trapping of Atoms," Ph.D. thesis, University of Colorado (1999).